Hannes BRANDNER, BSc

Modifying the Dielectric-Semiconductor Interface in Organic Thin-Film Transistors Using a Soluble Semiconducting Polymer

MASTER THESIS

For obtaining the academic degree
Diplom-Ingenieur

Master Programme of
Technical Physics

Graz University of Technology

Supervisor:
ao. Univ.-Prof. Dipl.-Ing. Dr.techn. Egbert ZOJER

Institute of Solid State Physics

Graz, February 2012

Contents

Acknowledgements

I want to thank my supervisor Egbert Zojer and my colleague Simon Außerlechner for guidance and advices throughout the work for this thesis.

I also appreciated the fruitful discussions and conversions with all members of the Zojer group (Ferdinand Rissner, David Egger, Marco Marchl, Lukas Ladinig, Reinhold Hetzel, Yao Shan, Martin Stolterfoht) that spiced up the usual day at the university.

Additionally I want to thank Alfred Neuhold and Roland Resel for their collaboration and support with the x-ray analysis.

Of course, I want to express my gratitude to Harald Kerschbaumer and Birgit Kunert who always were on the spot whenever help was needed in the laboratory. And I also want to thank Elisabeth Stern for her support with any administrative issues.

Financial support by the Austrian Science Fund (FWF): P 19959-N20 is acknowledged.

Kurzfassung

Die vorliegende Arbeit behandelt Grenzflächenmodifikationen von organischen Dünnfilmtransistoren (OTFTs) die das lösliche Polymer Poly(3-Hexylthiophen) als organischen Halbleiter verwenden. Der erste Teil der Arbeit handelt die wesentlichsten Grundlagen über OTFTs ab und beinhaltet weiters Beschreibungen über Röntgenmessmethoden, die zur Untersuchung von dünnen Schichten angewendet werden. Der zweite Teil beschreibt den Produktionsprozess zur Herstellung des jeweiligen OTFTs und wie die Messungen durchgeführt werden. Der dritte Teil beschäftigt sich mit der Auswertung der gewonnen Daten der unterschiedlichen Experimente. Zu Beginn werden die Eigenschaften eines einfachen Transistors besprochen, bei dem keine Modifiaktionen vorgenommen wurden. Anschließend werden Zwischenschichten eingeführt, die das vom Dielektrikum unabhängige Verhalten des organischen Halbleiters beobachtbar machen sollen. Weiters wird der Einfluss von säurehaltigen Grenzschichten auf die Parameter eines Transistors betrachtet. Zum Schluss wird noch das Intermixing von Polymeren, die aus orthogonalen Lösungsmitteln hergestellt werden, untersucht.

Abstract

The following thesis deals with interface modifications in organic thin-film transistors (OTFTs) that use a soluble polymer called poly(3-hexylthiophene) as organic semiconductor. The first part contains the basic theory about OTFTs. Then x-ray measurement techniques are described that are used to investigate thin-films. The second part covers all the information that concerns the production and electrical characterization of OTFTs. The third part deals with the evaluation of the experiments and measurements that have been conducted. At first, OTFTs with the simplest possible layout are discussed in detail and then interface modifications are introduced. These should enable the investigation of the genuine properties of the organic semiconductor, independent of the dielectric substrate. Later the influence of acidic interface layers on the properties of the OTFT are presented. The concluding chapter provides information about intermixing of orthogonally soluble polymers within an OTFT setup.

Chapter 1

Introduction

Low-cost, flexible, printable and large area applications - these are the buzzwords that are instantly associated with organic electronics. In recent years, a lot of effort has been put into research on new materials and production processes that can help to develop a new kind of technology, which some people think, is the future of electronics.

Organic solar cells, organic light emitting diodes (OLEDs) and OTFTs are the main 'players' in this new industry that is steadily growing. Especially OLEDs have emerged from the scientific level and entered everyday life. In the beginning, single OLEDs have been implemented in electronic devices, for example to show the status of the battery life in a razor [1]. But thanks to consumer electronics, OLED displays are nowadays widely known and desired for their outstanding brightness, contrast and clear imaging. At first it were only small applications such as simple cell phone displays which soon became touch-screen displays in smartphones [2]. Recently, television screens of several inches in diameter have been available and lately a 55 inch wide, 4 mm thin OLED screen has been presented[1]. These applications are not flexible because the driving electronic is still made of inorganic materials.

And here it comes to the implementation of OTFTs - organic thin-film transistors. Prototypes of flexible or even rollable displays[2] have been developed but until such electronic devices are ready for mass production, a lot of energy has to be put into research.

The organic semiconductor which is the basis of all organic electronics can either be made of small molecules or polymers. There is a wide range of different mate-

[1]LG electronics, January 2012, *www.lg.com/us/ces/index.jsp*
[2]Sony Corporation, May 2010, *www.sony.net/SonyInfo/News/Press/201005/10-070E/*

rials that are currently of interest. One specific polymer is poly-(3-hexylthiophene) (abbr.: P3HT). In recent years, our group has done a lot of research concerning this particular organic semiconductor and its implementation in OTFTs. The properties of P3HT-based OTFTs and ways to manipulate certain device characteristics have been investigated. But the production of polymers and the resulting properties strongly depend on the kind of synthesis that is used. Hence the 'behaviour' of an OTFT varies with every P3HT sample that is provided from a different supplier and often unfortunately also with different batches from the same supplier.

The last P3HT that was purchased by our group unfortunately did not work at all, although a lot of effort was put into making the OTFTs operational again. Nevertheless, it was impossible to build operating devices and that is why a new P3HT was bought from a new supplier: *Rieke Metals*.

The task at hand was to get the P3HT-OTFT production back on track and reproduce results that have been gathered before. After reaching these goals, new interface modifications had to be tested that should mainly result in manipulating one specific parameter, the threshold voltage.

Part I

Fundamentals

Chapter 2

Basic theory of OTFTs

The explanations contained in the following section are mainly based on the work from Brown et al. [3], Horowitz [4] and Newman et al. [5].

An organic thin-film transistor (OTFT) consists of basically five components:

- gate-electrode (G)
- source-electrode (S)
- drain-electrode (D)
- dielectric
- organic semiconductor (OSC)

There are four different ways to compose a OTFT out of these elements. One can either build top-gate bottom-contact, top-gate top-contact, bottom-gate bottom-contact or bottom-gate top-contact devices (see fig.2.1).

The distance between the source and drain electrode is the channel length L and the size of the electrodes determines the width W of the channel (fig. 2.2). The dielectric has a specific capacitance C that needs to be considered for any calculations that specify the performance of the transistor.

2.1 Working principle

In the following, the basic working principle of an OTFT is described. The first condition is that the organic semiconductor is of p-type, which means that the charge

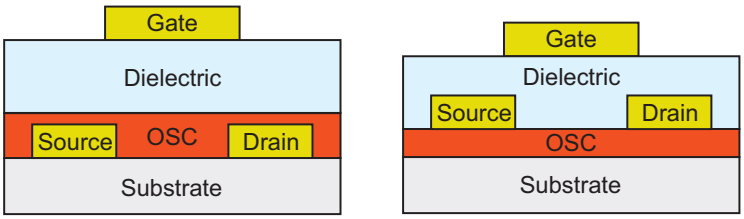

(a) top-gate bottom-contact

(b) top-gate top-contact

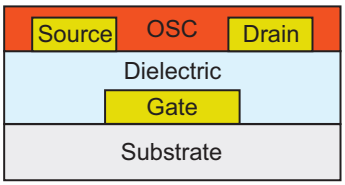

(c) bottom-gate bottom-contact

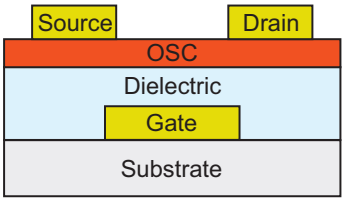

(d) bottom-gate top-contact

Figure 2.1: Device structures: 4 different arrangements of source-, drain- and gate-electrode, dielectric and organic semiconductor (OSC) on a substrate.

carriers are holes (instead of electrons in an n-type semiconductor). This is useful because the organic semiconductor at hand (P3HT) is operating like a p-type semiconductor due to the materials that are used as dielectric (silicon oxide) and electrodes (gold). Chua et al. [6] have shown that the choice of materials determines whether P3HT-OTFTs show p-type or n-type behaviour. The source electrode (V_S) is in any case grounded and the voltage at the drain (V_D) and gate (V_G) electrode can be varied.

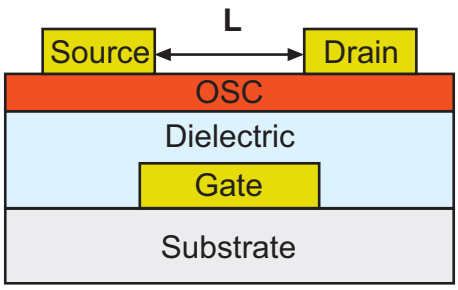

(a) Side view

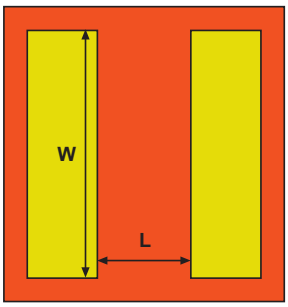

(b) Top view

Figure 2.2: Definition of channel width and length.

There is an additional parameter, the threshold voltage (V_T), which will be discussed later and is now assumed to be zero for the sake of simplicity.

Now one can systematically change the two variable voltages and discuss the charge carrier concentration in the organic semiconductor. The following explanations are supported by visualization in fig. 2.3.

The simplest case is that there is no voltage applied to the gate electrode. Due to the fact that the intrinsic charge carrier concentration in a semiconductor is very low, there is no conducting channel available between source and drain and, thus, the drain current $I_D = 0$ A, regardless of the voltage set to drain.

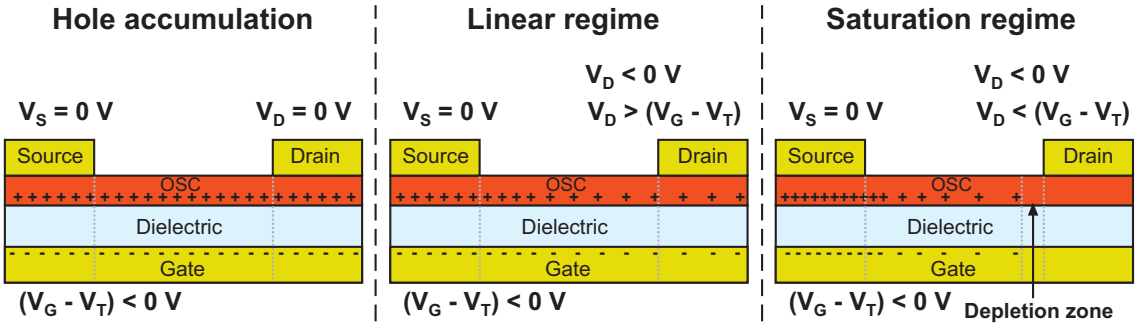

Figure 2.3: Visualized working regimes; V_T assumed to be 0 V;
Hole accumulation: holes are accumulated at the dielectric/semiconductor interface if $V_G < 0$ V and $V_D = 0$ V;
Linear regime: current between source and drain is linear dependent on V_G if $V_D > (V_G - V_T)$;
Saturation regime: current saturates and is now independent of V_D if $V_D < (V_G - V_T)$

If one applies a negative voltage to the gate while leaving $V_D = 0$ V, holes are accumulated at the dielectric/semiconductor interface and a homogeneous charge carrier distribution is formed which leads to a conducting channel between source and drain. Decreasing V_D to negative values but still fulfilling the condition $V_D > (V_G - V_T)$ causes a current flowing from source to drain. The drain current I_D is in this case linearly dependent on the applied gate voltage and can be described by the following equation:

$$I_{\mathrm{D}} = \frac{WC}{L}\mu\left[\left(V_{\mathrm{G}} - V_{\mathrm{T}}\right)V_{\mathrm{D}} - \frac{{V_D}^2}{2}\right] \tag{2.1}$$

W ... channel width
L ... channel length
C ... specific capacitance of dielectric
μ ... charge carrier mobility

A further decrease of the drain voltage leads to the so-called pinch-off, where $V_{\mathrm{D}} = (V_{\mathrm{G}} - V_{\mathrm{T}})$. Looking at the charge carrier distribution, this means that near the drain electrode a depletion zone is formed which completely lacks free holes. This region expands slightly further into the channel when $V_{\mathrm{D}} < (V_{\mathrm{G}} - V_{\mathrm{T}})$ [5]. Now the OTFT is operating in the saturation regime, where

$$I_{\mathrm{D}} = \frac{WC}{2L}\mu(V_{\mathrm{G}} - V_{\mathrm{T}})^2 \ . \tag{2.2}$$

One can see that the drain current now depends quadratically on V_G but it is completely independent of the applied drain voltage.

2.2 Charge transport

In contrast to metals or conventional semiconductors, there is no conduction band available that provides charge transport in organic semiconductors. Therefore, other possible mechanisms have to be considered to describe the occurrence of current in devices based on organic materials.

Hopping

The hopping-model is one possible theory to describe the charge transport in organic semiconductors. Charge carriers simply hop between localized states and do not undergo any transition to a delocalized state. This hopping is triggered by phonons in the organic semiconductor and is thus temperature dependent. The likelihood of hopping increases with the temperature and so does the charge carrier mobility.

This relation can be written as [4]:

$$\mu = \mu_0 \exp\left[-\left(T_0/T\right)^{1/\alpha}\right] . \tag{2.3}$$

α ... integer value of 1,2,3 or 4, depending on the type of the organic semiconductor

Multiple trapping and thermal release (MTR)

Alternatively, the charge transport can be described by the MTR-model. It assumes that there is in fact a transport band and a high concentration of localized states. The edge of the transport band (E_C) is considered to be close to the energy of the trap states (E_T). The charge carriers can now be thermally released into the transport band but will instantaneously be trapped again if they are in the vicinity of a trap. The effective mobility can then be written as [7]:

$$\mu_\mathrm{eff} = \mu_0 \alpha \exp\left[-\left(E_\mathrm{C} - E_\mathrm{T}\right)/kT\right] \tag{2.4}$$

μ_0 ... mobility in the transport band
α ... ratio of effective density of states at the transport band edge to the concentration of traps

2.3 Threshold voltage

In the previous subsection it was assumed that the threshold voltage equals zero, but generally this is not the case. For example the so-called flat-band voltage which accounts for the work-function difference between the organic semiconductor and gate [8] needs to be overcome. Another reason why V_T can differ from zero is that there are trap states that are filled before any charge carrier can contribute to a current. In p-type semiconductors such traps lead to negative threshold voltages.

Furthermore, unintended doping of the organic semiconductor by residual chemicals at the interface results in a shift of V_T to positive values [5].

Unfortunately, there is no uniquely accepted definition of V_T. Typically, it is treated as a parameter that is fitted from a characteristic and can be derived in many different ways [9]. In that sense it is not an intrinsic property of an OTFT.

2.4 Characteristics and parameter extraction

There are two different ways to characterize an OTFT. One can either sweep the gate-voltage and keep the drain-voltage constant ($\mapsto$ *transfer characteristic*) or sweep the drain-voltage and keep the gate-voltage constant ($\mapsto$ *output characteristic*). Generally, the sweep is performed in both directions, from positive to negative voltages (downward sweep) and back again (upward sweep). Examples of the characteristics are shown in fig. 2.4. The transfer characteristic in fig. 2.4(a) shows the

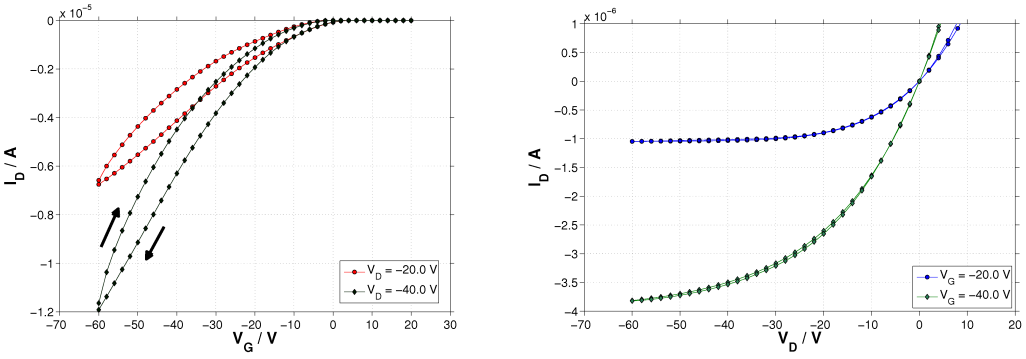

(a) Transfer characteristic

(b) Output characteristic

Figure 2.4: Characteristics that are used to determine the OTFT performance. (Displayed characteristics of an OTFT with P3HT on silicon dioxide and bottom-gate top-contact configuration)

appearance of a hysteresis which is attributed to trap states of the holes that contributed to the current in the downward sweep but became immobile in the upward sweep. On the other hand, the hysteresis is negligible in the output characteristic in fig. 2.4(b).

Although the mobility μ mentioned before was referred to as the charge carrier mobility, it is only an *effective* charge carrier mobility because the contact resistance is not taken into account when μ is simply extracted from the characteristic by

the fitting procedure described below (which are those typically used in literature). Furthermore, one has to distinguish between the evaluation of μ and V_{T} in the linear and in the saturation regime, as explained in the following paragraphs.

Linear regime

If one rewrites eqn. 2.1 as

$$I_{\mathrm{D}} = \frac{WC}{L}\mu\left[(V_{\mathrm{G}} - V_{\mathrm{T}}) - \frac{V_{\mathrm{D}}}{2}\right]V_D \tag{2.5}$$

it is obvious that when a straight line is fitted in this regime, at the intersection with the x-axes,

$$(V_{\mathrm{G}} - V_{\mathrm{T}} - V_{\mathrm{D}}/2) = 0 \ ,$$

needs to be fulfilled and V_{T} can be calculated. The effective charge carrier mobility μ can be extracted from the slope of the straight line. The resulting quantities shall be referred to as μ_{lin} and $V_{\mathrm{T,lin}}$.

Saturation regime

In this regime, the square root of eqn. 2.2 provides again a linear equation as a function of V_{G}:

$$\sqrt{I_{\mathrm{D}}} = \sqrt{\frac{WC}{2L}\mu}\,(V_{\mathrm{G}} - V_{\mathrm{T}}) \ . \tag{2.6}$$

If the transfer characteristic is now drawn in a square root plot, a straight line fitted in the saturation regime provides the data necessary to calculate $V_{\mathrm{T,sat}}$ and μ_{sat} (see fig. 2.5). The intersection with the x-axes shows now directly the threshold voltage but the mobility needs to be calculated from the squared slope.

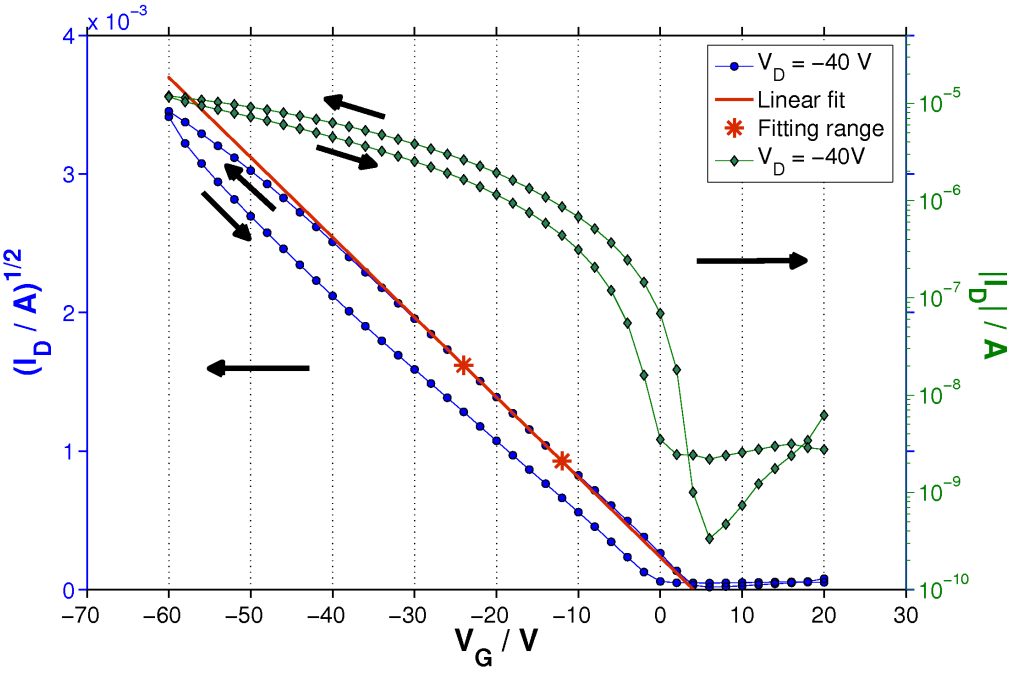

Figure 2.5: 'Square root plot' of the transfer characteristic with fitted straight line for parameter extraction together with logarithmic plot. (Displayed characteristics of an OTFT with P3HT on silicon dioxide and bottom-gate top-contact configuration)

On/off-ratio, V_{on}

In addition to the mobility and threshold voltage there are two other parameters that are useful to describe and compare the performance of OTFTs.

The on/off-ratio tells the order of magnitudes that lies between the drain current of a transistor that is switched on and a transistor that is switched off. This can be best seen in a logarithmic plot of the transfer curve (fig. 2.5). In order to make the ratio of different devices comparable, one has to add the information, which voltage range is covered by the on/off-ratio.

The turn-on voltage V_{on} simply shows at which voltage the drain current starts to increase significantly. This point can simply be extracted by finding the point with the steepest slope in the logarithmic plot (fig. 2.5).

In this work, all parameters of an OTFT are extracted from the downward sweep (V_{G} is changed towards negative values) of the transfer characteristic.

Chapter 3

X-ray analysis

The explanations contained in the following section are mainly based on the work from Kittel [10], Spieß [11] and Krumrey et al. [12]. Destruction-free methods to investigate the orientation and stacking of the organic molecules in a thin film as well as the film properties like layer thickness, layer roughness and electron density of the used material, are provided by x-ray analysis. In the context of this thesis, we have used three different investigation techniques to characterize the samples which shall now be briefly described.

3.1 X-ray diffractometry (XRD)

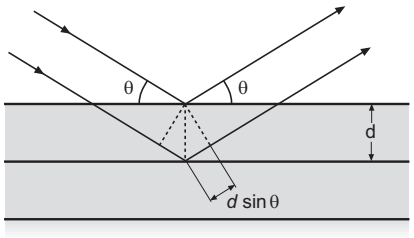

Figure 3.1: Schematic depiction of the Bragg-condition.

In crystals, there are repeating layers of atoms, that form the crystal structure. When x-ray photons hit the crystal, part of them are reflected at the surface and any parallel layer beneath the surface at the same angle as the incident ones (see fig. 3.1). There will only be a diffracted beam if the reflected rays add up constructively, which means that the path difference of the reflected x-rays has to be $n \cdot \lambda$, where λ is the

wavelength of the x-ray and $n = 1, 2, 3, ...$. This is only true if the Bragg-condition

$$n \cdot \lambda = 2d \sin\theta, \tag{3.1}$$

is fulfilled. Here d is the distance of the lattice planes and θ is the incident angle. Different lattice planes can be investigated by changing the incident angle as well as the detection angle. XRD measurements have been performed on the *PANalytical Empyrean* diffractometer using Cu_{K_α} radiation ($\lambda = 1.542$ $\AA$) provided by an laboratory x-ray tube.

3.2 Grazing incidence x-ray diffractometry (GIXD)

Grazing incidence x-ray diffraction is used to investigate the in-plane orientation of molecules in a thin film. This method characterizes crystallites with lattice planes lying rather perpendicular to the surface. In GIXD setup, the angle of the incident beam as well as the outgoing beam are kept at very small, constant values. This technique is extremely surface sensitive due to the fact that the incidence angle (ω) is set close to the critical angle of the investigated material. The measurement setup is based on a *Bruker D8 Discovery* diffractometer upgraded with the *Bruker Ultra GID* add-on. A schematic drawing of the measurement setup is shown in fig. 3.2.

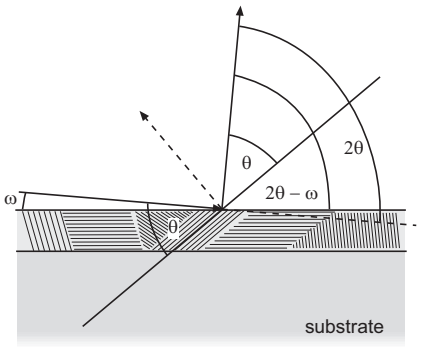

Figure 3.2: Schematic depiction of the GIXD principle: ω is the incidence angle of the x-ray in relation to the sample surface whereas θ is the angle between the incident beam and the crystallite's lattice planes (see also fig. 3.1). 2θ, respectively $2\theta - \omega$ is the angle between the diffracted beam and the extension of the incident beam. The detector is positioned in the direction of the outgoing beam; inspired by [11]

3.3 X-ray reflectometry (XRR)

X-ray reflectivity is a specular diffraction technique, where the incidence angle of the beam is equal to the angle of the diffracted beam (fig. 3.3). XRR uses the fact that the refractive index n of any material is less than unity and the phenomena of external total reflection occurs if the incidence angle of the beam is smaller than the critical angle of the material. The XRR method yields important quantities characterising thin films, like layer thickness, layer roughness and electron density.It is also useful for analysing multilayer arrangements. XRR measurements have been performed on the *PANalytical Empyrean* diffractometer. The measured XRR data have been simulated with the software package *X´Pert Reflectivity 1.3* (PANalytical) to extract the desired layer properties.

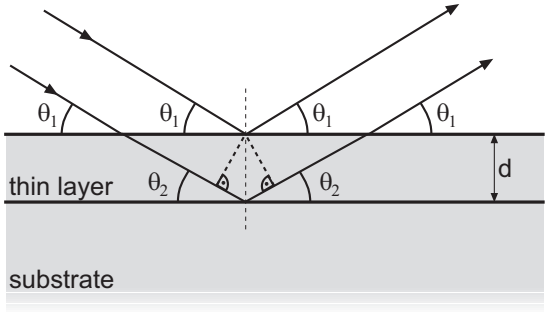

Figure 3.3: Schematic depiction of the XRR principle: θ_1 is the incidence and reflectance angle with respect to the sample surface. Due to the refractive index n of the thin film the direction of the transmitted beam is altered and it hits the substrate at an angle θ_2; inspired by [12]

Part II

Experimental

Chapter 4

Fabrication and device characterization

4.1 Organic semiconducting polymer rr-P3HT

The active layer that has been used for all the transistors built during the work for this thesis consists of the polymer regioregular-poly-(3-hexylthiophene)(in the following simply abbreviated as P3HT).

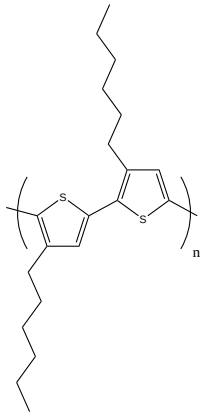

Figure 4.1: Structure of the semiconducting polymer regioregular-poly-(3-hexylthiophene); CAS: 156074-98-5

The polymer in use was purchased from Rieke Metal and has the product name *Sepiolid P200* (produced by BASF). The manufacturing company claims that the polymer is best soluble in chlorinated hydrocarbons and reasonably soluble in aromatic hydrocarbons. The regio-regularity of the polymer chain should also be higher

than 98 %, which means that the hexyl side chains linked to the thiophene backbone are fairly regularly oriented in the manner shown in fig. 4.1. In addition to that, it is stated that there is only a small trace of metals contained in the polymer and that mobilities up to 0.3 cm^2/Vs are possible. [13]

4.2 Production

All organic transistors have been built on heavily n-doped silicon substrates (phosphor as donor, ⟨100⟩-orientation, 1-20 Ωcm) with a thermally grown 150 nm thick silicon oxide layer purchased from Siegert Consulting e.K.. The substrates that have been used for the production have a size of two times two centimetres and contain four single transistors at the end of the fabrication process. In sec. 2 four different layouts of an OTFT are listed. During the whole work only the bottom-gate top-contact configuration has been used which can be seen in fig. 4.2.

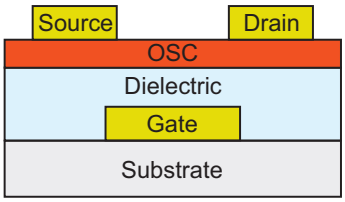

Figure 4.2: Bottom-gate top-contact design

Production steps

1. The substrates are only taken out of the packaging inside a laminar flow box to prevent the Si-wafers from unnecessary exposition to dust. After removing one substrate from the batch it is cleaned with a CO_2 spray.

2. Now the wafer is placed in an oxygen plasma etching chamber (fig. 4.3) where it is treated at maximum power for 30 s at a flowrate of 90% (100% = 90 cm^3/min; gauged with N_2 at 1.013 bar and 20°C) in order to get rid of residual dirt on top of the substrate and 'to reduce the traps at the SiO_x surface' [14]. Afterwards, the substrate is again cleaned with CO_2 and put into a Petri-dish.

Figure 4.3: Plasma etcher from *diener electronic* (model: *femto*) [15]

3. Optionally, an additional layer can now be put on the substrate (see sec. 4.4).

4. The Petri-dish is then transferred to the glove box where the deposition of solutions is carried out under argon atmosphere. The substrate is fixed with a double-faced adhesive tape to the dish of the spin coater which is custom built and driven by a cassette tape recorder motor (fig. 4.4). By simply changing the voltage that is applied to the engine one can tune the rotating speed. In the next step, 100 μl of the organic semiconducting material P3HT is deployed onto the substrate by spin-coating. The essential parameters at this point are the rotating speed of the dish and the spinning time. Due to the fact, that there has been done a lot of research in our working group with the mentioned polymer in recent years, the well established spinning parameters have not been changed. So the spin coater is driven by a supply voltage of 4 V and the P3HT is spin-coated for 40 s which results in a layer thickness of about 12 nm.

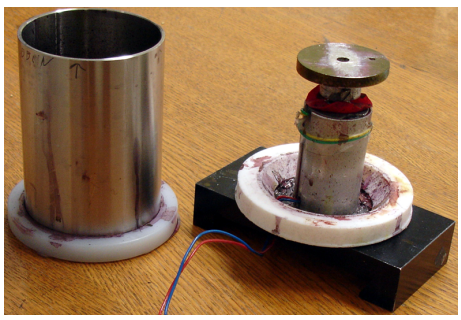

Figure 4.4: Self-made spin-coater

5. In order to get rid of the solvent in which the polymer has been dissolved, the sample is dried for 5 minutes at 80°C on a heating stage immediately after the

spin-coating process.

6. The sample is now transferred to another glove box, where the measurements are done and evaporation of metals or organic molecules is performed. In our case, the gold contacts need to be evaporated on the organic layer through a shadow mask (fig. 4.5), where a thin tungsten wire provides the gold-free channel between source and drain (fig. 4.6(b)). Finally, the channel length L equals 25 μm and the channel width $W = 7$ mm. In order to be able to contact the gate-electrode from the top of the substrate, one has to cut through the silicon oxide layer with a diamond-cuter. These scratches will later be covered with gold. The deposition of gold takes place at a pressure in the range of 1 to $2 \cdot 10^{-6}$ mbar which is measured close to the turbomolecular pump. Since the distance to the evaporation chamber is about one meter and a valve is positioned in between the actual pressure is likely to be one order of magnitude higher than 10^{-6} mbar. The gold is evaporated via an electrically heated tungsten boat and the thickness of the deposited gold layer is measured via a micro balance. The electrodes usually have a thickness of 50 nm.

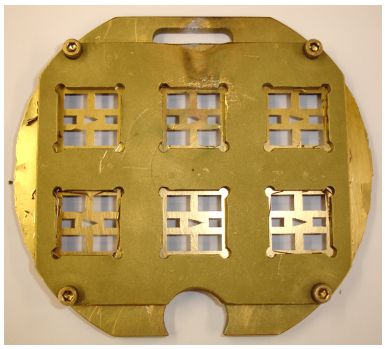

Figure 4.5: Shadow mask for gold deposition

The final result of the production process can be seen in fig. 4.6 along with an explanation of the individual elements. In order to distinguish the single transistors on one substrate from each other, a triangle of gold is also evaporated onto the substrate. With the triangle pointing upwards, the transistors and gate electrodes are now designated in a unique way (see fig. 4.6(c)). Furthermore, the substrates are numbered consecutively (H_1, H_2, H_3, ... H_159).

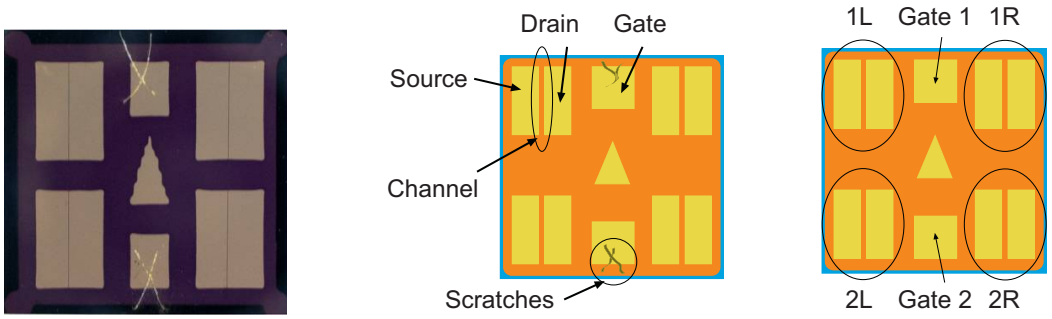

(a) Real device (b) Description of device (c) Nomenclature

Figure 4.6: Scheme of finished substrate and real device

4.3 Device characterization

The electronic characterization of the organic transistors produced with the shadow mask shown in fig. 4.5 can either be carried out with test prods (fig. 4.7(a)) or a home-built measuring cell (fig. 4.7(b)).

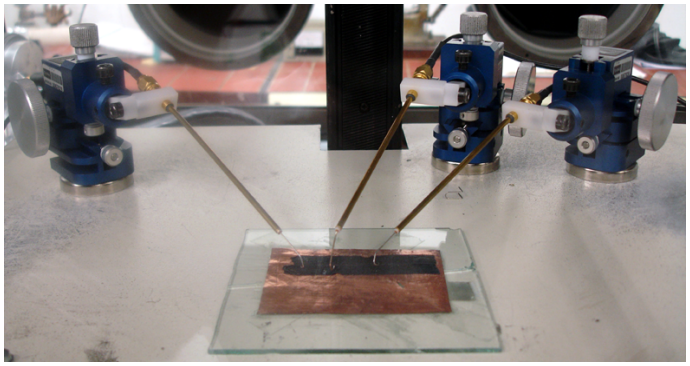

(a) Test prods

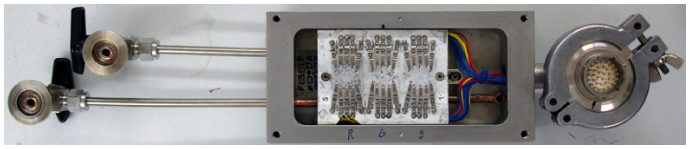

(b) Measuring cell

Figure 4.7: Measurement equipment.

The three electrodes source, drain and gate are connected to a Keithley KE2623A unit (fig. 4.8(a)), which is controlled via a LabView application that has been programmed by Thomas Obermüller, a former group member. Three substrates can be

inserted into the measuring cell at once and each of the electrodes are contacted separately. Via three switches(fig. 4.8(b)) one can easily choose between the different transistors on the substrates. This is a huge advantage compared to the test prods, because one has to contact the electrodes only once before starting the measurement procedure. This saves a lot of time when many transistors need to be characterized.

(a) Keithley 2623A source-measure unit

(b) Switch of measuring cell

Figure 4.8: Measuring tools

The transfer (and output) measurement starts at the voltage $V_{\mathrm{G,start}}$ ($V_{\mathrm{D,start}}$) and is then changed by a voltage step of $V_{\mathrm{G,step}}$ ($V_{\mathrm{D,step}}$) towards negative values. There is a delay time of 0.1 s in between these steps. The downward sweep stops at a specified voltage $V_{\mathrm{G,end}}$ ($V_{\mathrm{D,end}}$) and is subsequently followed by the upward sweep from $V_{\mathrm{G,end}}$ ($V_{\mathrm{D,end}}$) to $V_{\mathrm{G,start}}$ ($V_{\mathrm{D,start}}$) with the same voltage steps and delay time.

These sweeps are performed several times before the characteristic, which is used for evaluation, is taken.

4.4 Interface modifications

In order to modify the transistor's parameters, an additional layer can be inserted, for example, in between the SiO_x and the P3HT layer. Five different interface modifications have been tested in the course of this thesis:

n-hexadecyltrichlorosilane

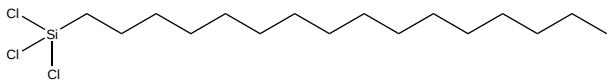

Figure 4.9: Structure of n-hexadecyltrichlorosilane; CAS: 5894-60-0; purchased from ABCR GmbH;

This is a molecule (see fig. 4.9) which forms a so called self-assembled mono-layer (SAM) that is intended to passivate the surface of the wafer. Since it docks to the SiO_x with the trichlorosilane group the hydrophobic tail of the molecule forms the new interface on which the P3HT is deployed.

At production step 3 of sec. 4.2, one has to do the following to build a passivation layer of $n - hexadecyltrichlorsilane$ (HDTS):

The substrate is cleaned in a supersonic bath for 2 min in de-ionized water (18 MΩcm H_2O). Afterwards it is dried by a spray of CO_2. Now the substrate, and two cleaned and warm bottles which have been stored in an oven at 80°C for at least 14 hours, are transferred into the glove box.

One bottle gets filled with 10 ml and the other with 6 ml anhydrous toluene with a syringe. The substrate is now put into the bottle which contains 10 ml toluene and then 10μl of HDTS (pure substance) are added to the bottle using a pipette (which should be held vertical and touch the bottle's wall with its tip).

The substrate is kept in the closed bottle with the solution for 16 h and afterwards put in the bottle with the 6 ml of toluene to stop the self-assembling process. Now the wafer needs another supersonic bath which means that it has to be put out of the glove box again. This time it is kept in the toluene during the 2 min lasting supersonic treatment. Before the substrate is dried with CO_2, some fresh toluene is rinsed over it to remove any loose residual HDTS. The next step is to dry the wafer

in a vacuum chamber (evacuated with a rotary vane pump) at 80°C for 30 min and let it cool down in vacuum for another 2 h. To finish the production process, steps 4 to 6 listed in section 4.2 are applied.

T-SC/SA

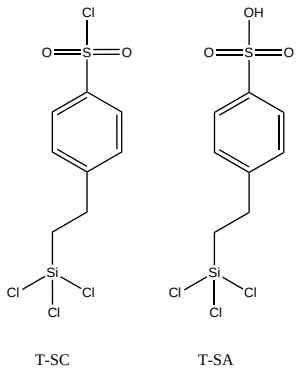

Figure 4.10: Structure of 4-(2-(trichlorosilyl)ethyl)benzene-1-sulfonyl chloride (T-SC) and 4-(2-(trichlorosilyl)ethyl)benzene-1-sulfonyl acid) (T-SA); CAS: 79793-00-3; purchased from ABCR GmbH;

T-SC/SA (fig. 4.10) is again a SAM-material containing 70% of T-SC and 30% of T-SA but its purpose is completely different compared to the one of HDTS. Instead of passivating the surface and revealing the genuine properties of P3HT, the acidic component of the T-SC/SA dopes the P3HT and thus forms a space charge layer due to the acidic residuals (see fig. 4.11). This results in a well pronounced positive shift of the threshold voltage [16]. A theoretical study to confirm the origins of this effect was done by Possanner et al. [17] and the results of their simulations support the previous assumption.

The production steps to create a self-assembled mono-layer are the same as for HDTS. Only the duration of the wafers in the T-SC/SA/toluene solution is changed to 30 min which is sufficient to create a proper T-SC/SA layer. It has to be added that the T-SC/SA is delivered as a solution of 50% in toluene. Instead of adding 10 μl of pure substance, 10 μl of this solution are added to 10 ml toluene.

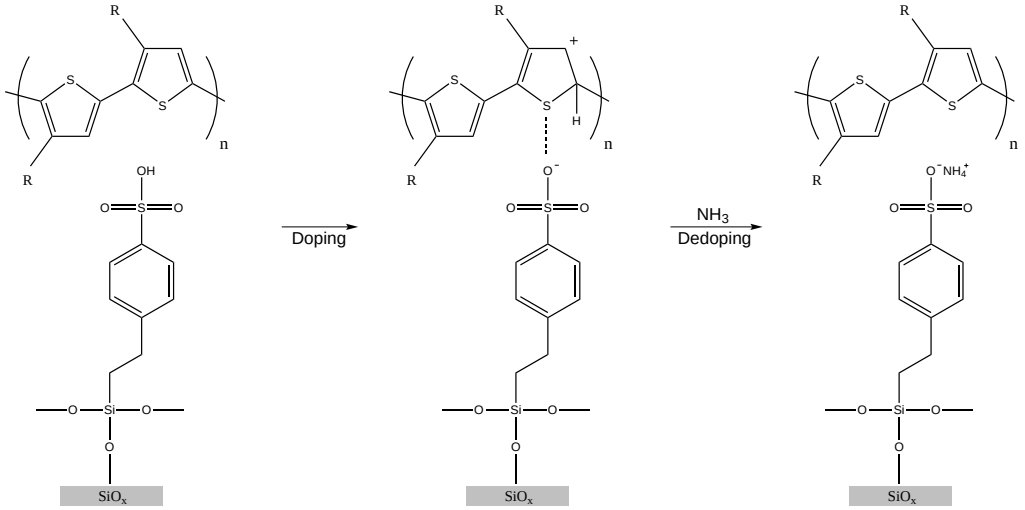

Figure 4.11: Doping and de-doping mechanism of T-SA

poly(4-styrenesulfonic acid)

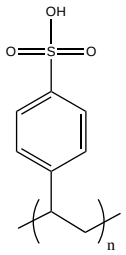

Figure 4.12: Structure of poly(4-styrenesulfonic acid); CAS: 28210-41-5; purchase from Sigma Aldrich;

poly(4-styrenesulfonic acid) (PSSA, see fig. 4.12) is a polymer that is soluble in water and should provide qualitatively the same results as the T-SC/SA layer because it has the same functional group as the T-SA molecule. Since PSSA is a polymer that can simply be deposited by spin coating onto the substrate the corresponding layers are faster, easier and (keeping industrial applications in mind) cheaper to produce.

Again, after production step 3 of sec. 4.2, the following procedure has to be applied to create a PSSA layer of about 10 nm:

Using a PSSA solution which has a concentration of 3.6 mg PSSA / 1 ml H_2O, the spin coating is done under ambient conditions in the already mentioned flow

box. 150 μl of the solution are put on the substrate by a pipette and then spread by spinning the sample for

- 15 s at 2000 rpm followed by
- 40 s at 3500 rpm.

The spin coater used for this procedure is shown in fig. 4.13. The two different times and speeds are programmed before the sample is placed on the dish, where it is secured by a vacuum suction nozzle.

Afterwards the PSSA layer can optionally be heated in a vacuum chamber for 2 h and further cooled for 1.5 to 2 hours. The impact of this optional treatment on the transistor will be discussed later.

Now one has to follow production steps 4 to 6 in sec. 4.2, in order to finish the transistor.

Figure 4.13: Spin coater from *Chemat Technology* (model: *KW-4A*) used inside the flow box;

poly(acrylic acid)

poly(acrylic acid) (PAA, see fig. 4.14) is another water soluble polymer that is intended to shift the threshold voltage of a P3HT based transistor when inserted at the SiO_x-P3HT interface, as it also leaves acidic groups.

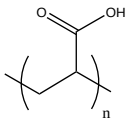

Figure 4.14: Structure of poly(acrylic acid); CAS: 9003-01-4; purchased from Sigma Aldrich

Except for the concentration of the polymer in water, which should now be 5 mg PAA / 1 ml, and the spin parameters that are changed to

- 9 s at 1000 rpm followed by
- 40 s at 4000 rpm,

the production steps are the same as for the PSSA.

4.5 Gas exposure

Some transistors have eventually been exposed to a gas, in order to cause a change of the organic transistor's parameters. This section will provide some information about how a transistor is exposed to a specific gas. The effects of the gas on an OTFT will be discussed in chapter 7.

Ammonia (NH_3):
The exposure of an OTFT to ammonia gas can be performed without any exposure to ambient air because it is done via the closed measuring cell shown in fig. 4.7(b).

The measuring cell is equipped with a gas supply pipe and an exhaust pipe, which allows the user to have any gas flow through the cell. At first the supply pipes are purged with argon. Then the cell is flushed with ammonia gas at a pressure of 1.5 bar and a flow rate of 9 l/h for 5 min (the exposure time can vary according to the samples or purpose of the exposure) and afterwards the residual NH_3 is blown out with argon gas to stop the exposure of the sample to ammonia. Furthermore, this shall prevent the pollution of the glove box, where the cell will be opened again and of course avoid a possible poisoning of any person handling the cell. Therefore the whole procedure is done in a fume hood.

Part III

Evaluation

Chapter 5

Reference devices

The organic semiconductor P3HT that has been used for this work was delivered from a new supplier. Therefore its performance and response to bias stress and light had to be tested. The following section deals with these tests.

5.1 P3HT on SiO_x

The simplest possible design of an OTFT - organic semiconductor on dielectric - has been used as reference for any modifications that were done throughout the whole work of this thesis. In this particular case it means that a 10 to 12 nm thin layer of P3HT dissolved in chloroform was deposited on a 150 nm thick layer of silicon oxide. The arrangement can be seen in fig. 5.1.

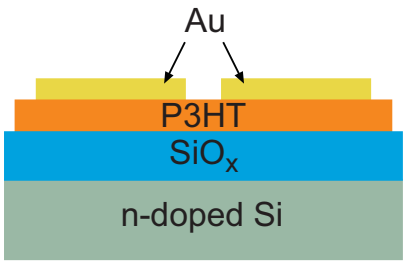

Figure 5.1: Layout of a reference device.

The performance of these reference devices has been investigated in different ways and the effects of a different pretreatment of the substrates were studied as well.

Generally, the transistors were measured in argon atmosphere and with laboratory lights on. The effective charge carrier mobility of a reference device is in the range of 10^{-3} cm^2/Vs. Only a small amount of transistors have a mobility which is one order of magnitude lower. The threshold voltage is generally within a few volts in the range of zero. The performance is reasonably good reproducible. The characteristics of one exemplary transistor are shown in fig. 5.2 and its parameters are listed in tab. 5.1.

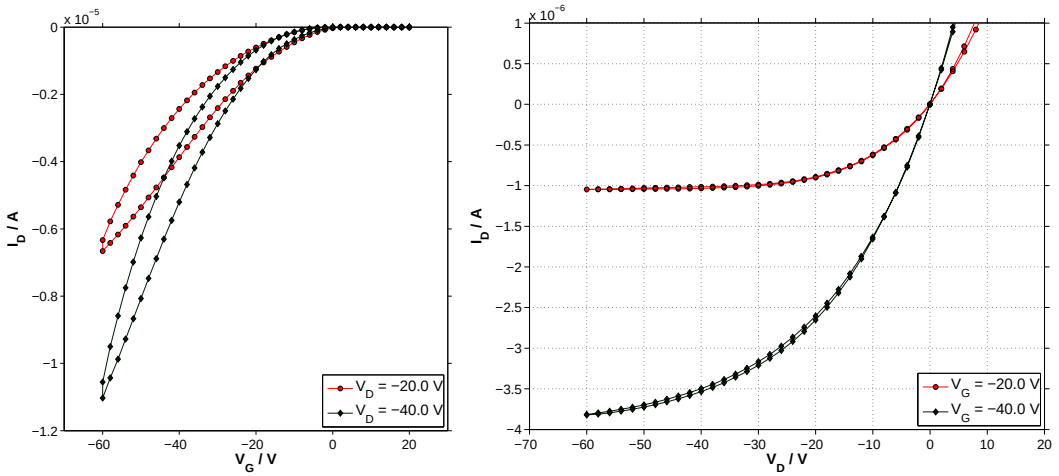

(a) Transfer characteristic (b) Output characteristic

Figure 5.2: Characteristics of a reference OTFT; OTFT nr. H_15 1R.

Table 5.1: Properties of device H_15 1R from fig. 5.2(a)
V_D ... applied drain voltage, μ_{sat} ... effective charge carrier mobility (fitted in saturation regime), $V_{T,sat}$ ... threshold voltage (fitted in saturation regime)

V_D / V	μ_{sat} / cm^2/Vs	$V_{T,sat}$ / V
-20	$0.74 \cdot 10^{-3}$	3.6
-40	$1.02 \cdot 10^{-3}$	-1.0

One can see clearly that the transfer characteristics that have been measured at different drain voltages match reasonably well down to about V_G = -20 V where the linear regime of the transfer curve that has been measured at V_D = -20 V begins. This result fits quite well to the theory which states that in the saturation regime, the drain current is completely independent of the applied drain voltage.

Another feature that can be seen in fig. 5.2(a) is the hysteresis that is relatively

large. As described in sec. 2 trap states at grain boundaries or the semiconductor/dielectric interface are responsible for its appearance.

The characteristics of a transistor are always measured one week after the production because investigations have shown that one day after the production the transistors show low mobility and large hysteresis whereas the performance has clearly improved after 12 days (see fig. 5.3 and tab. 5.2). This can maybe attributed to an ordering process of the polymer chains or better charge carrier injection due to oxidation of the gold electrodes [18].

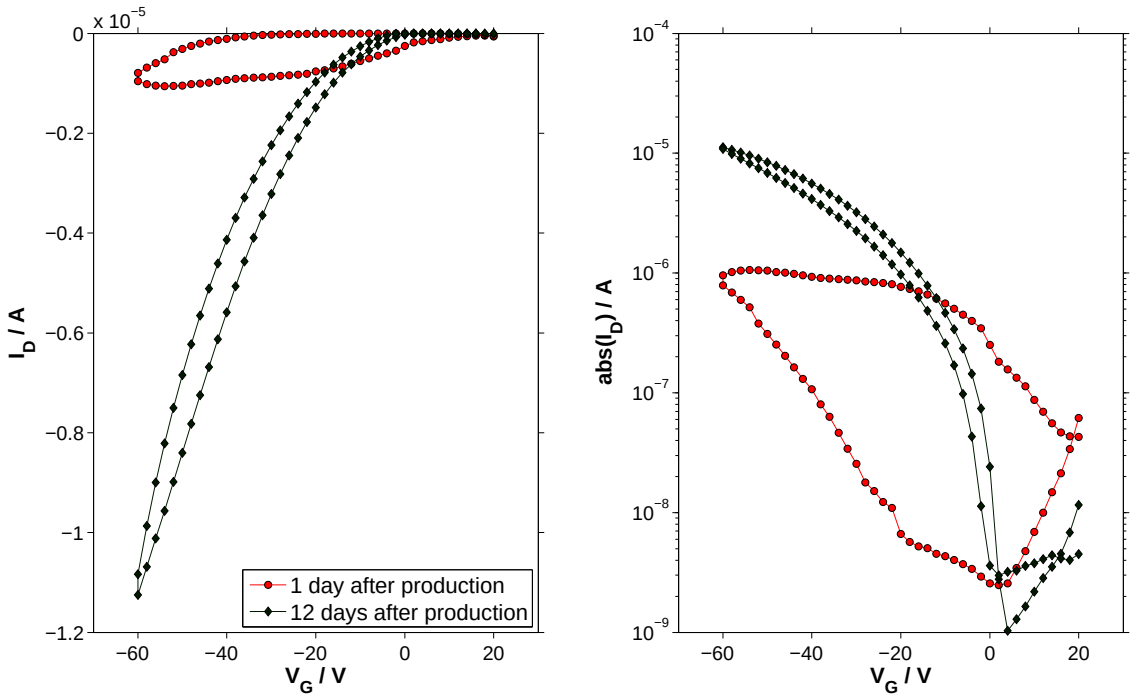

Figure 5.3: Transfer characteristic of a reference device 1 and 12 days after the production; V_D = -40;
OTFT nr. H_12 1R.

Table 5.2: Properties of device H_12 1R from fig. 5.3
V_D ... applied drain voltage, μ_{sat} ... effective charge carrier mobility (fitted in saturation regime), $V_{T,sat}$ ... threshold voltage (fitted in saturation regime)

measured after	V_D / V	μ_{sat} / 10^{-3}cm^2/Vs	$V_{T,sat}$ / V
1 day	-40	0.3	-33
12 days	-40	1.0	1.1

5.1.1 Shelf life of OTFTs

All devices have been stored in a glove box under argon atmosphere for the whole time. Since the shelf life of OTFTs can always be an issue, the performance of a reference OTFT has been monitored over a time period of 2 months. It has to be added that the oxygen and moisture sensor of the glove box were malfunctioning over the whole time period. Therefore it is ambiguous how high the concentration of water and oxygen was during the investigation. The results in fig. 5.4 show that after one month the device reaches its best performance, regarding the mobility and hysteresis of the transistor. But after two months the characteristics are almost as good as one month before, which indicates that the degeneration of the devices takes place slowly. The most important thing is though that only after about one week, the transistor is working properly and improves only slightly in the following weeks as can be seen in tab. 5.3.

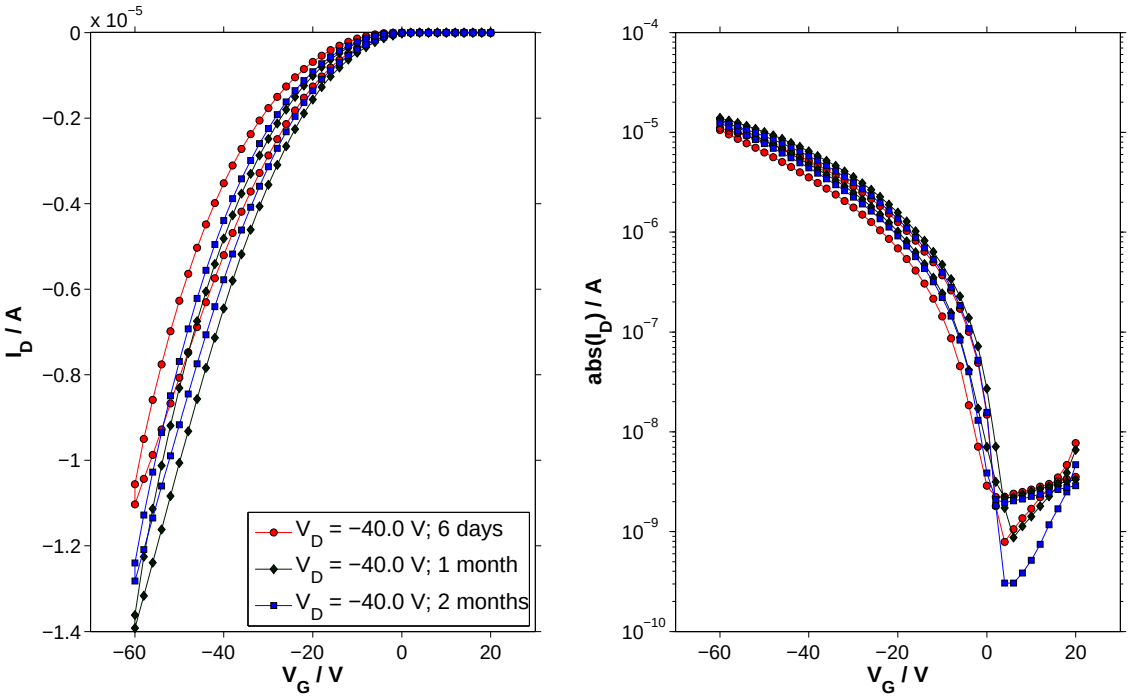

Figure 5.4: Performance development of a reference device within 2 months; OTFT nr. H_15 1R.

Table 5.3: Properties of device H_15 1R from fig. 5.4
V_D ... applied drain voltage, μ_{sat} ... effective charge carrier mobility (fitted in saturation regime), $V_{T,sat}$ ... threshold voltage (fitted in saturation regime)

measured after	V_D / V	μ_{sat} / $10^{-3}cm^2/Vs$	$V_{T,sat}$ / V
6 days	-40	1.0	-1.0
1 month	-40	1.3	-1.0
2 months	-40	1.2	-2.0

5.1.2 Bias stress

During testing the OTFTs the measurement range was systematically changed in order to investigate the response to a positive gate bias. The gate voltage sweeps always cover a range of 80 V and the voltage step is set to 2 V with a delay time of 0.1 s. The first measurement starts at V_G = 20 V and reaches down to V_G = -60 V, the second one starts at 30 V and reaches down to -50 V and so on, up to a start voltage of V_G = 60. The results are displayed in fig. 5.5 and tab. 5.4. They reveal that if the range is shifted towards more positive values, V_T is shifted too.

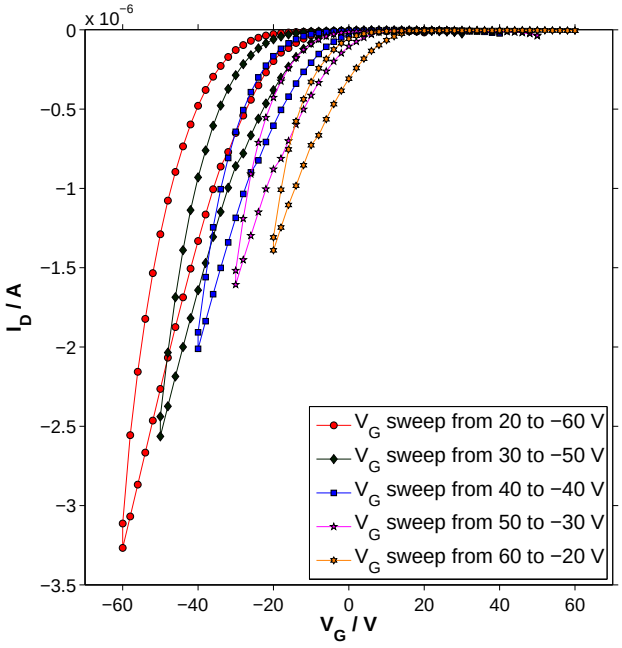

Figure 5.5: Transfer characteristics of a reference device at different measurement ranges leading to a threshold voltage shift; V_D = -40;
OTFT nr. H_70 1L.

Table 5.4: Properties of device H_70 1L from fig. 5.5
V_D ... applied drain voltage, μ_{sat} ... effective charge carrier mobility (fitted in saturation regime), $V_{T,sat}$ ... threshold voltage (fitted in saturation regime)

meas. range	V_D / V	μ_{sat} / $10^{-3}cm^2/Vs$	$V_{T,sat}$ / V
20 to -60 V	-40	0.40	-8.7
30 to -50 V	-40	0.38	-3.9
40 to -40 V	-40	0.35	1.6
50 to -30 V	-40	0.33	8.3
60 to -20 V	-40	0.31	17.1

A negative gate bias shifts the threshold voltage back to its initial value.

This well pronounced threshold voltage shift is attributed to electrons that are trapped at the P3HT/SiO_x interface. Chua et al. [6] reported that at high positive gate voltages electrons are injected from the gold electrodes into the organic semiconductor and trapped by silanol groups on the SiO_x surface. Hence, the negatively charged space charge layer causes the positive V_T shift (see fig. 5.6). But fortunately, this effect is completely reversible.

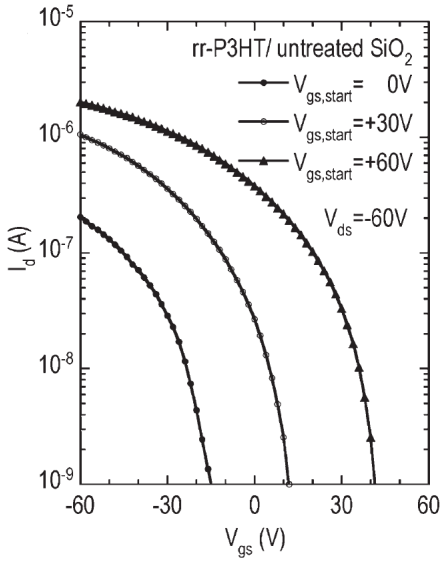

Figure 5.6: Bias stress: P3HT on SiO_x; figure taken with permission from [6].

5.1.3 Influence of light

In the course of getting to know the new P3HT's behaviour when used in an OTFT, the influence of light on a device was investigated. The initial trigger to do so came from our group member Simon Außerlechner who found, that the effect of interface modifications can be strongly affected by the absence/presence of light in an OTFT based on the organic semiconductor pentacene (fig. 5.7).

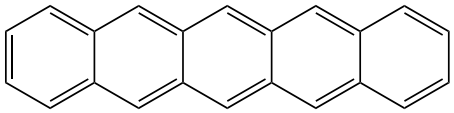

Figure 5.7: Structure of the semiconducting small molecule pentacene; CAS: 135-48-8.

Based on this information it was evident that the reaction of a reference OTFT made from P3HT to light illumination needed to be examined.

For this reason, a reference device has been protected from light since the last step of the production. Its Petri-dish was wrapped in aluminium foil and during the transfer from the evaporation chamber into the measuring cell and back, it was only exposed to light emitted from red LEDs. The LEDs needed to be turned on to provide at least a little bit of light in order to handle the substrates properly. The measurements however were performed in utter darkness, because the measuring cell can be sealed completely. The device was measured after 2 weeks in the dark, followed by two hours of illumination by the laboratory lights and a subsequent measurement in light.

Table 5.5: Properties of device H_106 1R from fig. 5.8
V_D ... applied drain voltage, μ_{sat} ... effective charge carrier mobility (fitted in saturation regime), $V_{T,sat}$ ... threshold voltage (fitted in saturation regime)

measured	V_D / V	μ_{sat} / $10^{-3}cm^2/Vs$	$V_{T,sat}$ / V
before illumination / in the dark	-40	0.2	-28
after 2 h illumination / in the light	-40	0.3	7

The results show that the threshold voltage is shifted several ten volts to negative values (fig. 5.8) when the OTFT is measured in the dark. This rather well pronounced effect has also been reported by Jing et al. [19] and they state that 'the light directly stimulates more carriers' and 'the effect of light can be viewed as an equivalent to a large gate bias'. In other words the light de-traps trapped holes.

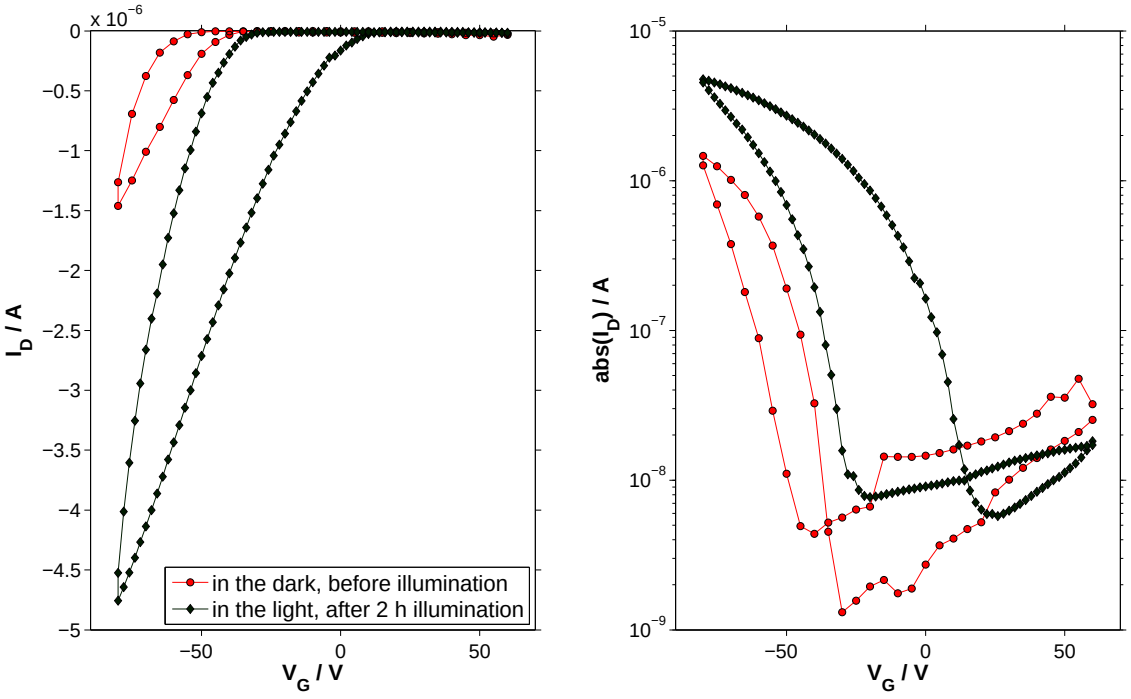

Figure 5.8: Transfer characteristic of a reference device measured in the dark before illumination and after 2 hours in light; V_D = -40;
OTFT nr. H_106 1R.

The effect of light on the OTFT can be reversed by putting it in the dark again. After two months without any light, the device was measured in the dark again. The positive threshold voltage shift caused by the light has vanished (see fig. 5.9 and tab. 5.9).

It has not been investigated how much time it takes to reverse the influence of the light. It can simply be stated that at least after two months storage in complete darkness the characteristic is shifted back again towards negative values.

Table 5.6: Properties of device H_106 1R from fig. 5.9
V_D ... applied drain voltage, μ_{sat} ... effective charge carrier mobility (fitted in saturation regime), $V_{T,sat}$ ... threshold voltage (fitted in saturation regime)

measured	V_D / V	μ_{sat} / 10^{-3}cm^2/Vs	$V_{T,sat}$ / V
before illumination / in the dark	-40	0.2	-28
after 2 h illumination / in the light	-40	0.3	7
after 2 months w.a.l. / in the dark	-40	0.4	-33

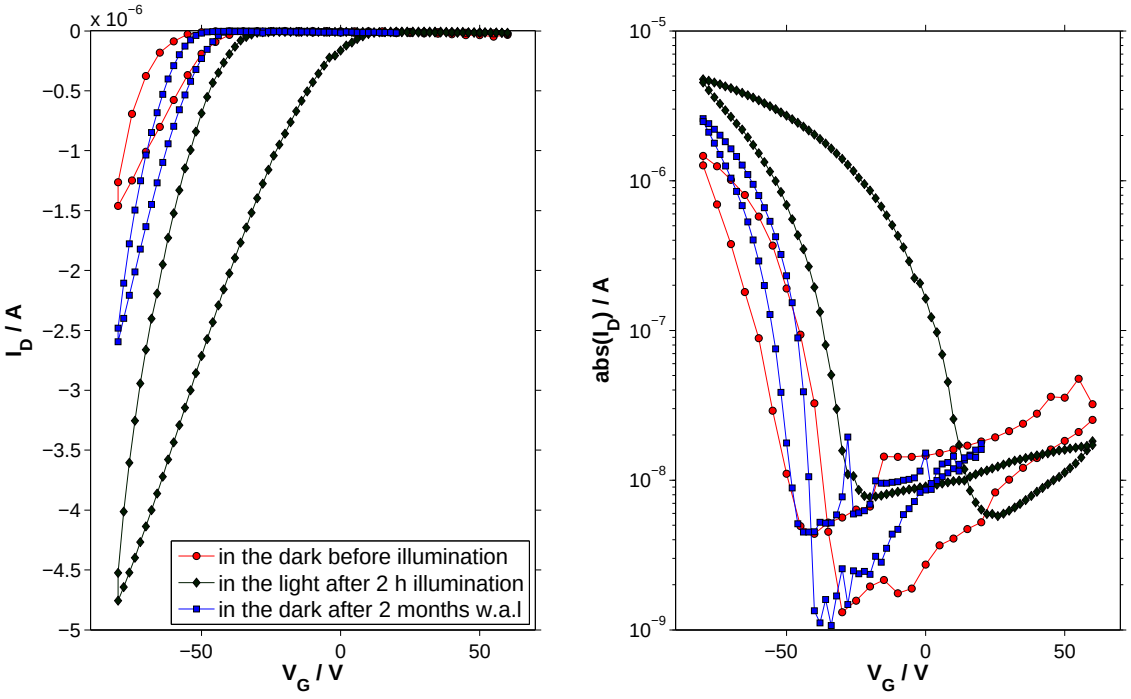

Figure 5.9: Transfer characteristic of a reference device measured in the dark before illumination, after 2 hours in light and after 2 months without any light (w.a.l.); V_D = -40;
OTFT nr. H_106 1R.

5.1.4 P3HT on heated silicon dioxide substrate

The reference devices exhibit a rather large hysteresis which is a bit disturbing. The cleaning process of plasma etching makes the silicon oxide surface more hydrophilic than it was before. The fact that the presence of water has a negative influence on the hysteresis of an OTFT [20] leads to the idea to heat the substrate prior to the deposition of P3HT.

Consequently some substrates have been heated in vacuum up to 120°C for one hour and then cooled down before the P3HT was spin coated onto them. Since the vacuum chamber with the heating stage was inside an argon filled glove box, the exposure of the substrates to water after the heating process was reduced to a minimum.

As one can see in fig. 5.10, the comparison between a reference device and an

OTFT with a heated substrate reveals that the additional heating does not have any effect on the hysteresis at all and μ_{sat} and $V_{T,sat}$ do not change significantly either (see tab. 5.7)

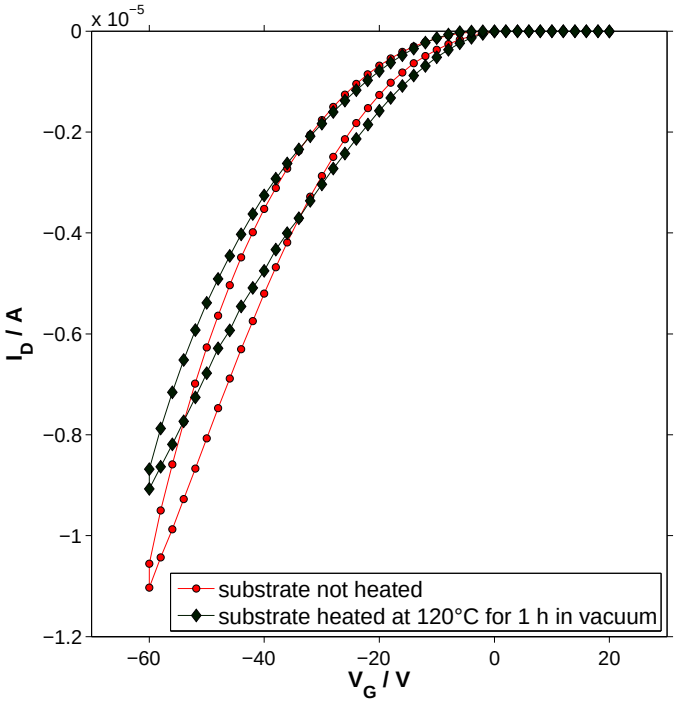

Figure 5.10: Comparison of transfer characteristics between usual reference OTFT and reference OTFT whose substrate was heated for one hour at 120°C in vacuum prior to deposition of P3HT; V_D = -40;
OTFT nr. H_15 1R (not heated) and H_146 1L (heated).

Table 5.7: Properties of device H_15 1R and H_146 1L from fig. 5.10
V_D ... applied drain voltage, μ_{sat} ... effective charge carrier mobility (fitted in saturation regime), $V_{T,sat}$ ... threshold voltage (fitted in saturation regime)

treated	V_D / V	μ_{sat} / 10^{-3}cm^2/Vs	$V_{T,sat}$ / V
not heated	-40	1.0	-1.04
120°C for 1 h in vac.	-40	1.1	1.92

5.2 Conclusion

The investigations on reference devices have shown that the P3HT at hand can provide reasonably good OTFT parameters for a semiconducting polymer. Nevertheless, it is crucial to keep an eye on the measurement conditions such as light and bias stress because they very significantly influence the device behaviour.

On the other hand, it appears that the production process does not bring in a lot of water into the devices, because the results of the device with a substrate heated prior to the P3HT deposition do not show any improvement in the OTFT characteristics.

A possible way to enhance the performance of the devices is the annealing of the P3HT layer before or after the gold evaporation at high temperatures. As several works [21–24] have shown, annealing at high temperature after the spin coating process improves the performance. Anyway, this treatment was not suitable in this case because the future work involved additional polymer layers on the substrate that needed to be deposited before the spin coating of the P3HT. Heating at high temperature could have led easily to a destruction or strong interaction between the two polymer layers. Furthermore, if one simply skips the annealing process for stacked polymer layers but still applies it to the reference devices, a comparison of the results is not useful.

Chapter 6

P3HT on passivation layers

In order to observe the performance of an OTFT that is less dependent on the silicon dioxide dielectric, one has to insert an additional layer between it and the organic semiconductor. In this thesis two different passivating interface modifications have been tested.

6.1 P3HT on n-hexadecyltrichlorosilane

As already described in sec. 4.4, HDTS forms a layer that provides a hydrophobic interface for the P3HT. This should reduce the amount of water in the transistor and also shield the charge carriers from trap states that are usually caused by the SiO_x surface. This specific material was used because it is similar to a molecule that was discussed by Pernstich et al. [25] amongst several other interface modifications and because it has been used before in our group and seemed appropriate to be test with the new P3HT. The new layout of the OTFT is shown in fig. 6.1.

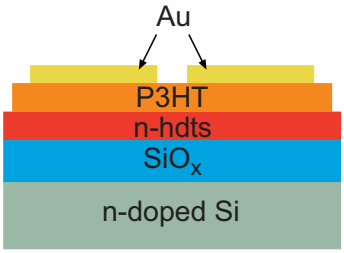

Figure 6.1: Layout of an OTFT with a passivation layer made of HDTS.

The characteristics of such a modified device are displayed in fig. 6.2 and its most important parameters are listed in tab. 6.1. The hysteresis in the transfer characteristic is very narrow and in the output characteristic it is hardly noticeable.

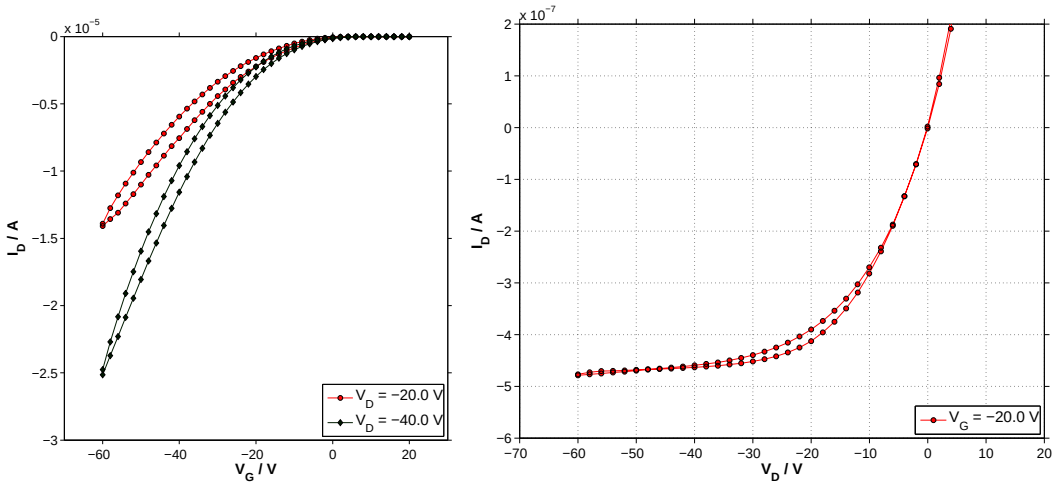

(a) Transfer characteristic (b) Output characteristic

Figure 6.2: Characteristics of an OTFT modified with HDTS; OTFT nr. H_17 1L.

Table 6.1: Properties of device H_17 1L from fig. 6.2
V_D ... applied drain voltage, μ_{sat} ... effective charge carrier mobility (fitted in saturation regime), $V_{T,sat}$ ... threshold voltage (fitted in saturation regime)

V_D / V	μ_{sat} / cm^2/Vs	$V_{T,sat}$ / V
-20	$1.01 \cdot 10^{-3}$	5.7
-40	$2.19 \cdot 10^{-3}$	-0.4

The effect of the passivation layer can best be seen in fig. 6.3 where the performance of a modified device is compared to a reference device.

The most prominent effects are that the hysteresis is clearly reduced and that the charge carrier mobility is slightly improved (tab. 6.2). On the other hand, the threshold voltage is not affected by the new interface although the logarithmic plot suggests that V_T is several volts higher in the HDTS-modified transistor. But the 'square root plot' in fig. 6.4 reveals that the fitted lines in fact intersect the x-axis nearly at the same point. In fact, the subthreshold regime in the OTFT with the

passivation layer is larger than in the reference device which is due to trap states (see Kane [26]).

The reduced hysteresis can be attributed to less residual water which means fewer long living trap states, whereas the increased mobility is believed to arise from a better morphology of the deposited P3HT that is promoted by the new surface. Unfortunately, no x-ray analysis has been done on these samples. Nevertheless the results are in good agreement with the findings of Pacher et al. in [16].

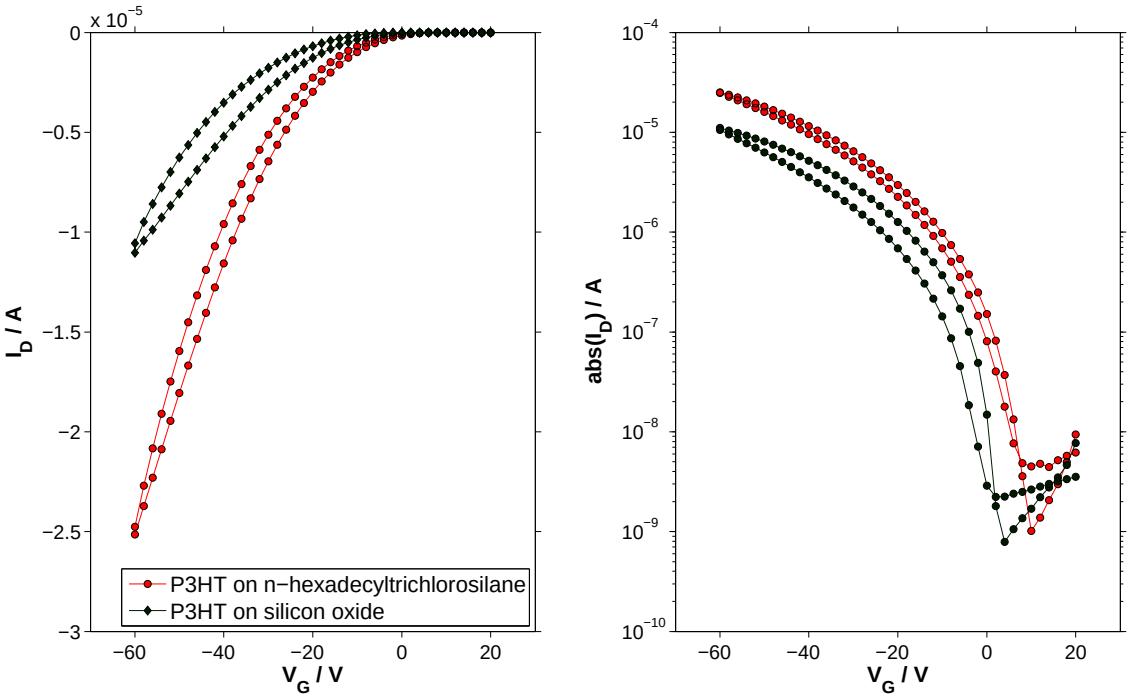

Figure 6.3: Transfer characteristics of an OTFT with P3HT on a passivation layer made of HDTS compared to a reference device; V_D = -40;
OTFT nr. H_17 1L (HDTS) and H_15 1R (reference).

Table 6.2: Properties of device H_17 1L (HDTS) and H_15 1R (reference) from fig. 6.3
V_D ... applied drain voltage, μ_{sat} ... effective charge carrier mobility (fitted in saturation regime), $V_{T,sat}$ ... threshold voltage (fitted in saturation regime)

layout	V_D / V	μ_{sat} / 10^{-3}cm^2/Vs	$V_{T,sat}$ / V
P3HT on HDTS	-40	2.2	-0.4
P3HT on SiO_x	-40	1.0	-1.0

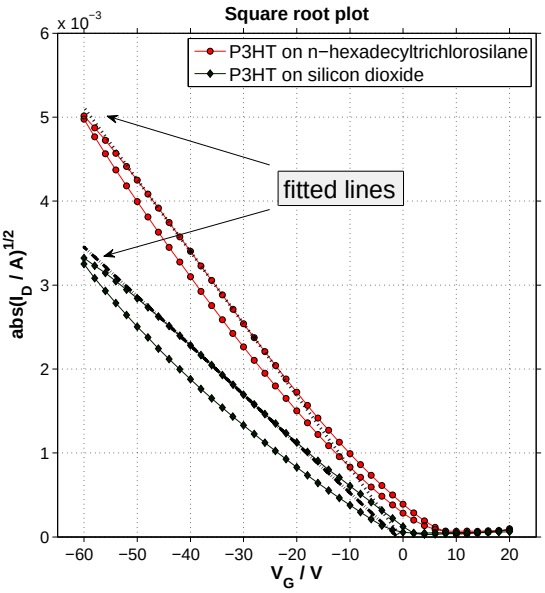

Figure 6.4: 'Square root plot' of the transfer characteristics of an OTFT with P3HT on a passivation layer made of HDTS compared to a reference device and their according fitted lines; V_{D} = -40;
OTFT nr. H_17 1L (HDTS) and H_15 1R (reference).

6.1.1 Bias stress

As we are dealing with a new layout, the effect of bias stress needs to be discussed again. The same measuring routine as in sec. 5.1 has been applied to OTFTs containing the HDTS layer. The starting voltage of the transfer characteristic sweep is changed from 20 to 60 V and a very well pronounced shift of $V_{\mathrm{T,sat}}$ is observable (see fig. 6.5 and tab. 6.3). It seems like the additional layer does not prevent the electrons to be trapped at the silicon dioxide or the HDTS surface.

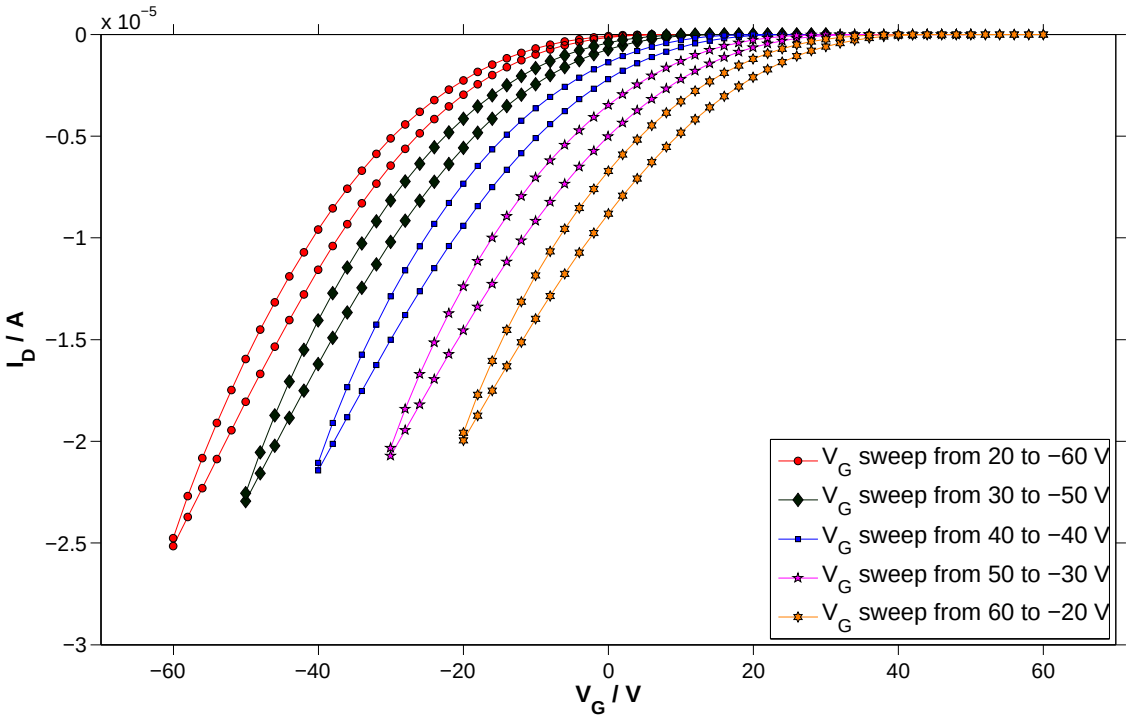

Figure 6.5: Transfer characteristics of an OTFT with P3HT on a passivation layer made of HDTS at different measurement ranges; stress induced threshold voltage shift is visible; all transfer curves measured at V_D = -40 V;
OTFT nr. H_17 1L.

Table 6.3: Properties of device H_17 1L from fig. 6.5
V_D ... applied drain voltage, μ_{sat} ... effective charge carrier mobility (fitted in saturation regime), $V_{T,sat}$ ... threshold voltage (fitted in saturation regime)

meas. range	V_D / V	μ_{sat} / 10^{-3}cm^2/Vs	$V_{T,sat}$ / V
20 to -60 V	-40	2.19	-0.4
30 to -50 V	-40	2.06	8.4
40 to -40 V	-40	1.96	17.8
50 to -30 V	-40	1.85	28.4
60 to -20 V	-40	1.78	38.5

6.2 P3HT on hexamethyldisilazane

In comparison to the HDTS another passivation layer has been used to study the genuine properties of the P3HT.

A thin layer of hexamethyldisilazane (HMDS, fig. 6.6(b)) has been deposited onto the silicon oxide by Kerstin Schmoltner at the research facility *Nanotec Center Weiz*.

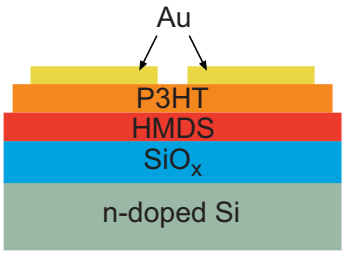

(a) Layout of an OTFT with a passivation layer made of HMDS.

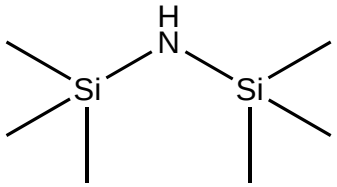

(b) Structure of HMDS; CAS: 999-97-3.

Figure 6.6: OTFT with HMDS.

HMDS is widely used to improve the performance of OTFTs based on P3HT (e.g. see [6], [27] and [28]). The new layout is shown in fig. 6.6(a).

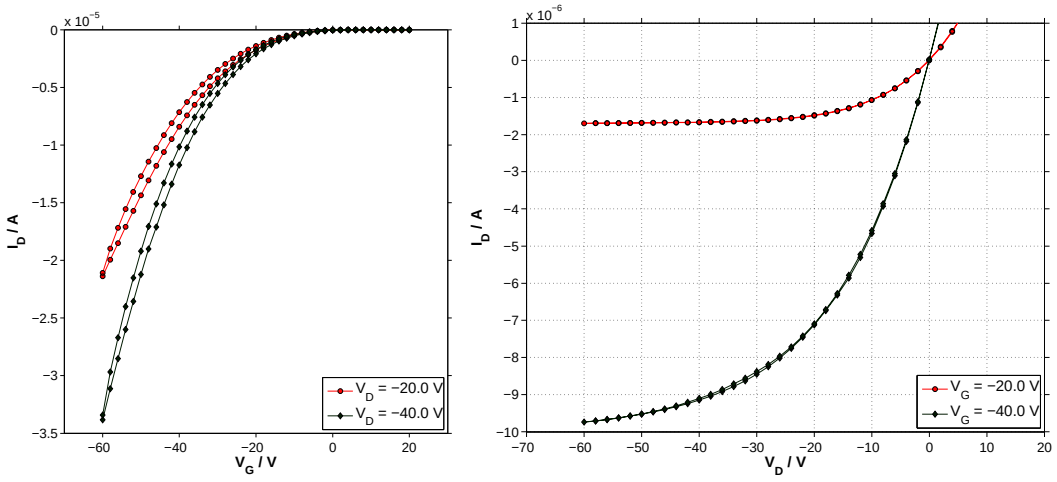

(a) Transfer characteristic

(b) Output characteristic

Figure 6.7: Characteristics of an OTFT modified with HMDS; OTFT nr. H_134 1L.

The characteristics of a device with P3HT on HMDS are shown in fig. 6.7. The performance has improved even compared to the HDTS devices. There is now only a very narrow hysteresis and the mobility is further increased (see tab. 6.4). This improvements can be explained by the promoted self-organisation of the P3HT chains on top of the HMDS layer [28].

The hysteresis in the output characteristic is again negligible.

Table 6.4: Properties of device H_134 1L from fig. 6.7
V_D ... applied drain voltage, μ_{sat} ... effective charge carrier mobility (fitted in saturation regime), $V_{T,sat}$ ... threshold voltage (fitted in saturation regime)

V_D / V	μ_{sat} / cm^2/Vs	$V_{T,sat}$ / V
-20	$3.75 \cdot 10^{-3}$	1.9
-40	$4.10 \cdot 10^{-3}$	-10.8

A direct comparison between a reference and an HMDS-modified OTFT shows the dramatic differences of these two device setups (see fig. 6.8 and tab. 6.5). In addition to the better alignment of the P3HT molecules the hydrophobic interface that is provided by the HMDS layer may contribute to the enhanced performance.

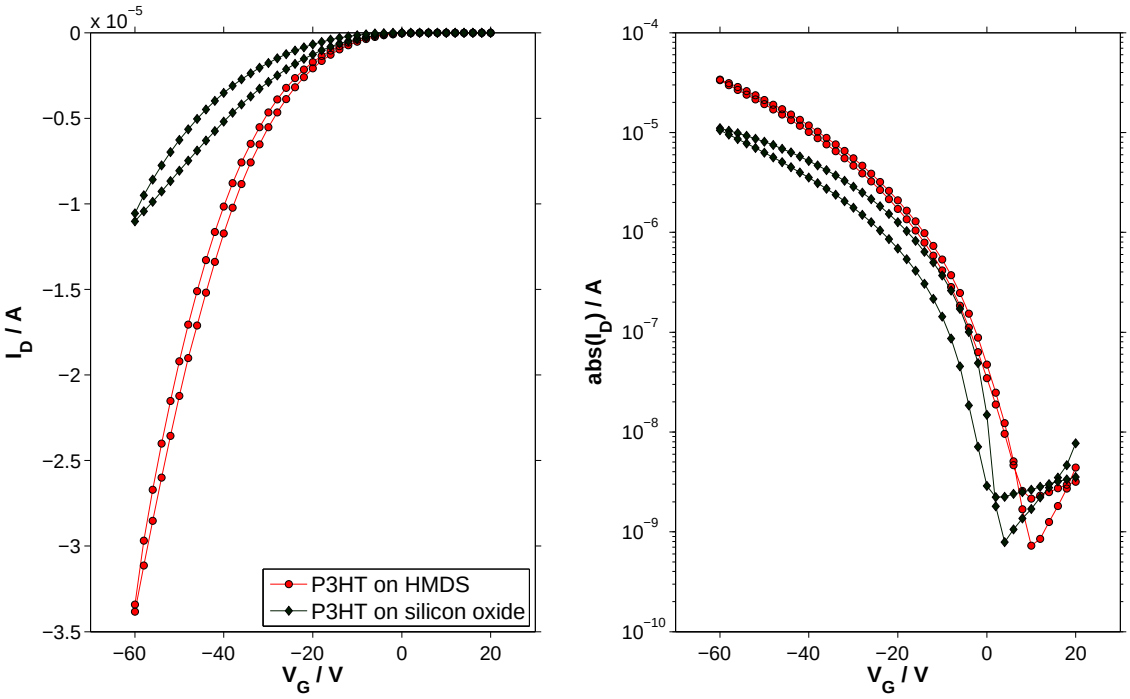

Figure 6.8: P3HT on a passivation layer made of HMDS compared to a reference device; V_D = -40; OTFT nr. H_134 1L (HMDS) and H_15 1R (reference).

Table 6.5: Properties of device H_134 1L (HMDS) and H_15 1R (reference) from fig. 6.8
V_D ... applied drain voltage, μ_{sat} ... effective charge carrier mobility (fitted in saturation regime), $V_{T,sat}$ ... threshold voltage (fitted in saturation regime)

layout	V_D / V	μ_{sat} / $10^{-3}cm^2/Vs$	$V_{T,sat}$ / V
P3HT on HMDS	-40	4.1	-11
P3HT on SiO_x	-40	1.0	-1.0

6.2.1 Bias stress

Again the bias stress effect was investigated with this OTFT layout. The same measuring routine as in sec. 5.1 has been applied to OTFTs containing the HMDS layer. The results are shown in fig. 6.9 and tab. 6.6. In the first three gate voltage sweeps the threshold voltage changes just by eight volts but above a start voltage of $V_G = 40$ V it changes significantly.

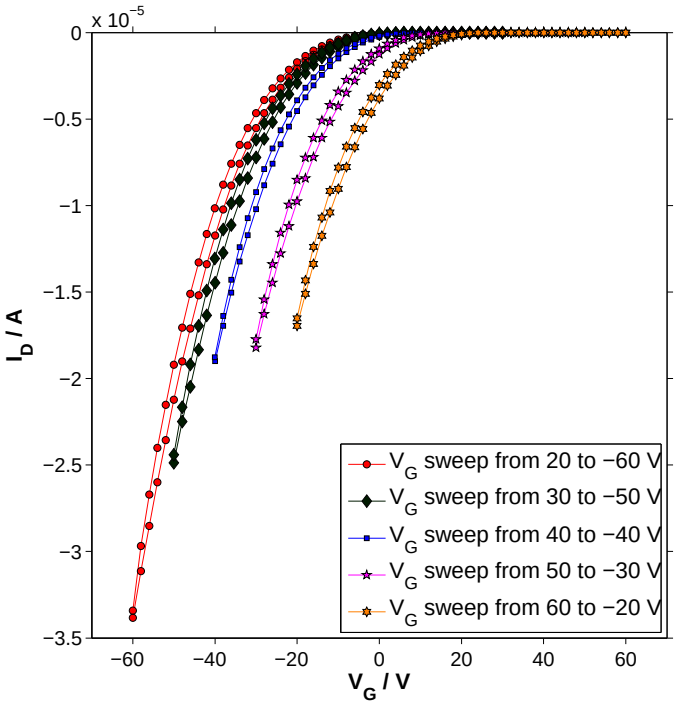

Figure 6.9: Transfer characteristics at different measurement ranges of an OTFT modified with HMDS, all transfer curves measured at V_D = -40 V;
OTFT nr. H_134 1L.

Unfortunately this is not the behaviour that has been expected according to the results that are published by Chua et al. in [6] and Sirringhaus in [20]. With an

Table 6.6: Properties of device H_134 1L from fig. 6.9
V_D ... applied drain voltage, μ_{sat} ... effective charge carrier mobility (fitted in saturation regime), $V_{T,sat}$ ... threshold voltage (fitted in saturation regime)

meas. range	V_D / V	μ_{sat} / 10^{-3}cm^2/Vs	$V_{T,sat}$ / V
20 to -60 V	-40	4.10	-10.8
30 to -50 V	-40	4.22	-8.0
40 to -40 V	-40	4.03	-2.6
50 to -30 V	-40	3.86	7.4
60 to -20 V	-40	3.67	17.0

HMDS-treated substrate one observes hardly any change of the threshold voltage, even when the gate voltage sweep starts from 60 V (fig. 6.10).

Also in our measurements it appears that the HMDS can prevent the electrons from being trapped at the SiO_x interface at lower positive gate voltages but above a start voltage of $V_G = 40$ V the complete curve shifts significantly (see fig. 6.9 and tab. 6.6).

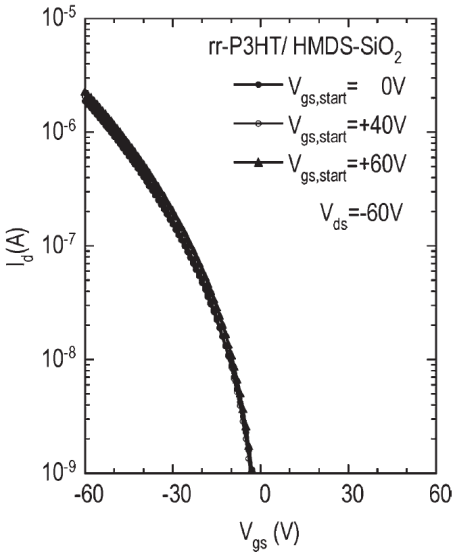

Figure 6.10: Bias stress: P3HT on HMDS (on SiO_x); figure taken with permission from [6].

6.3 Conclusion

The two passivation layers that have been presented in this chapter improve the overall performance of a P3HT transistor. A better mobility and less pronounced hysteresis are the most significant achievements.

The only aspect that diminishes the positive impact of the two materials is that the bias stress effect is still present at an extent that was not expected. The additional layers are not able to prevent the electrons from getting trapped at the silicon oxide surface.

Maybe the thickness of the passivation layers is not sufficient. Another explanation could be that the strong response to bias stress is simply a property of the P3HT at hand. The latter is a rather devastating assumption.

An interesting experiment that has not been carried out during this thesis is a test of the influence of light on an OTFT with a passivation layer. It would be interesting to know whether the tremendous shift of the whole transfer curve also occurs in a device with such an interface modification. This is an experiment that should be conducted in the future.

Chapter 7

P3HT on acidic layers

7.1 P3HT on T-SC/SA

As already discussed in sec. 4.4, a SAM made of T-SC/SA inserted between the dielectric and P3HT layer (see. 7.1) dopes the polymer chains and forms a space charge layer at the interface.

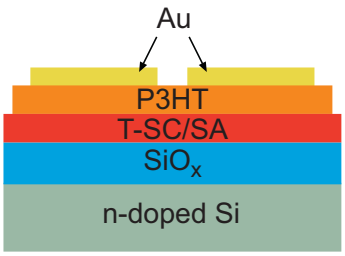

Figure 7.1: Layout of an OTFT with a SAM made of T-SC/SA.

As a result, the threshold voltage is shifted towards more positive values. Our group has done some research with this OTFT configuration in the past when the devices used to be fabricated with P3HT that was provided from another supplier. The according characteristics are shown in fig. 7.2.

One can see that the threshold voltage of an OTFT with T-SC/SA as active layer is shifted several ten volts to positive values and that the device is not turned off even at $V_G = 60$ V. The threshold voltage shift can be undone by exposing the transistor to pure ammonia gas, which neutralises the space charge layer and

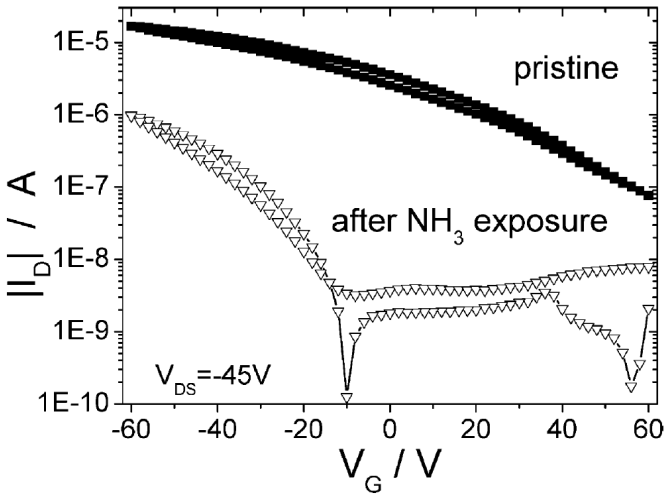

Figure 7.2: Transfer characteristic of a pristine P3HT/T-SC/SA OTFT and transfer characteristic after exposure to NH_3; figure taken with permission from [16];

de-dopes the organic semiconductor as shown in sec. 4.4, fig. 4.11. In fact, V_T can be tuned by mixing NH_3 and Ar and thus change the concentration of the ammonia gas. The higher the ratio of NH_3 to Ar, the larger is the threshold voltage shift in the negative direction. This behaviour has been investigated in detail by Etschmaier et al. [29].

In order to confirm that the new P3HT can be doped as well and shows the same behaviour as the previous P3HT, this interface modification was done again with the new organic semiconductor. The results of the experiment are shown in fig. 7.3. It has to be mentioned that the transfer characteristics had to be done at higher drain voltages because the devices used to get short-circuited now and then if they where measured at e.g. V_D = -40 V.

The threshold voltage was in this case evaluated in the linear regime, because the saturation regime was to small to get sufficient data for fitting the parameters (see tab. 7.1).

Although the fitted threshold voltage is below 60 V, the curves in fig. 7.3(a) suggest that the transistor is not even turned off at 60 V. However, there is a kink in the transfer characteristics that occurs in the vicinity of the saturation regime in every device that is modified with T-SC/SA. The origin of this feature is unknown by now.

A comparison of the transfer characteristics in fig. 7.3(a) and fig. 7.2 shows that

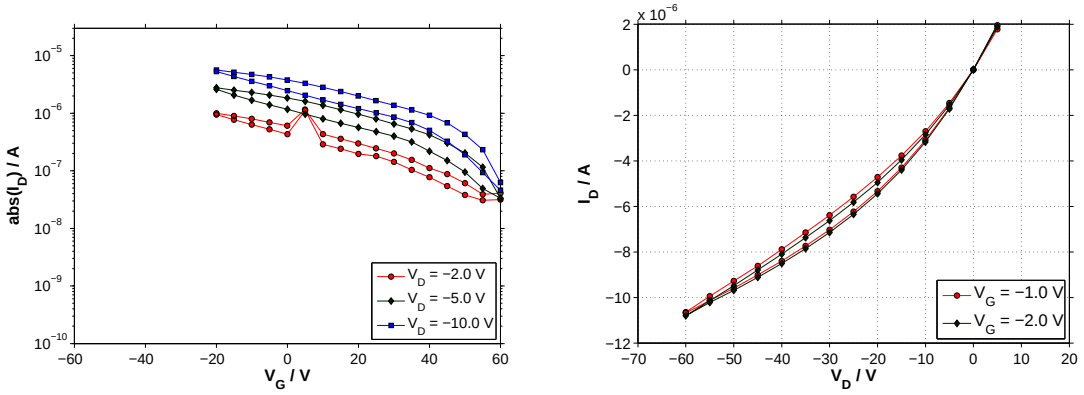

(a) Transfer characteristic (logarithmic plot) (b) Output characteristic

Figure 7.3: Characteristics of an OTFT modified with T-SC/SA;
OTFT nr. H_46 1R.

the hysteresis is larger in the T-SC/SA devices built from the new P3HT and the curves start with a steeper slope.

The output characteristic in fig. 7.3(b) only shows two different curves in the linear regime although the applied gate voltages are high compared to output characteristics of reference devices. Because of the tremendous positive threshold voltage the gate voltage should be some ten volts higher in order to observe the saturation regime in the same measurement interval of V_D. However, such output characteristics have not been recorded although these measurements could reveal at which certain point the device starts to saturate and whether it actually saturates at all. At the time these experiments were carried out it was not of utter importance to study the behaviour of this OTFT layout in great detail. As mentioned above, it should simply reproduce the results of former investigations.

Table 7.1: Properties of device H_46 1R from fig. 7.3(a)
V_D ... applied drain voltage, μ_{sat} ... effective charge carrier mobility (fitted in linear regime), $V_{T,sat}$ ... threshold voltage (fitted in linear regime)

V_D / V	μ_{lin} / cm^2/Vs	$V_{T,lin}$ / V
-2	$1.4 \cdot 10^{-3}$	40
-5	$1.4 \cdot 10^{-3}$	41
-10	$1.4 \cdot 10^{-3}$	44

7.1.1 De-doping with ammonia gas

Since it has been shown that the doping process of P3HT with T-SC/SA works as expected it needed to be verified that the de-doping mechanism works too. The treatment of the device with NH_3 was performed as described in sec. 4.5. The OTFT was exposed to pure ammonia gas for 1 min and measured four hours after the treatment. The characteristics in fig. 7.4 show a shift of the transfer curve in negative direction and the fitted threshold voltage in the linear regime changes by about forty volts as can be seen in tab. 7.2. The effective charge carrier mobility slightly decreases but is still of the same order of magnitude.

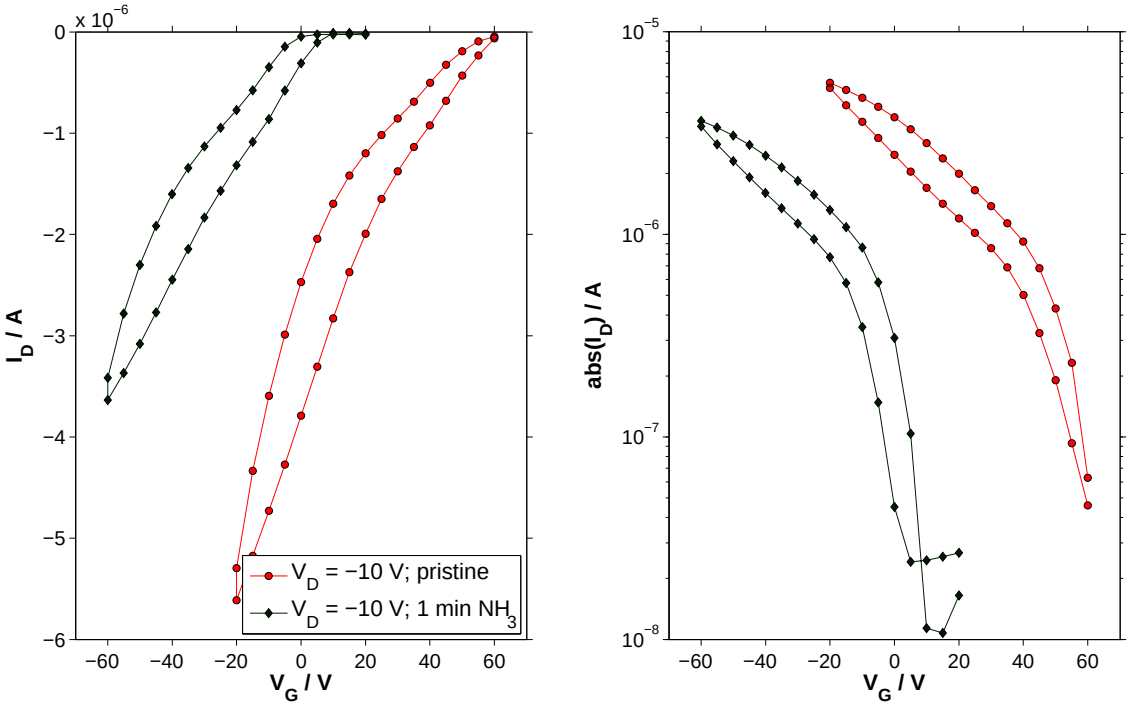

Figure 7.4: Transfer characteristics of an OTFT with T-SC/SA before and after 1 min enduring exposure to ammonia gas;
OTFT nr. H_46 1R.

With these results at hand it can be stated that the characteristic of the NH_3 treated OTFT resembles a reference device. Furthermore, the hysteresis and the shape of the two curves in fig. 7.4 are almost the same and this fact fits the findings of Possanner et al. [17] which again reinforces the conclusion that the doping and de-doping of the new P3HT and the organic semiconductor material itself is functioning accurately. Hence, new experiments can be conducted.

Table 7.2: Properties of device H_46 1R from fig. 7.4
V_D ... applied drain voltage, μ_{sat} ... effective charge carrier mobility (fitted in linear regime), $V_{T,sat}$ ... threshold voltage (fitted in linear regime)

treatment	V_D / V	μ_{lin} / 10^{-3}cm^2/Vs	$V_{T,lin}$ / V
pristine	-10	1.4	44
NH_3	-10	0.9	4

7.1.2 Influence of light

As already mentioned in sec. 5.1, Simon Außerlechner discovered that light significantly influences the behaviour of pentacene based OTFTs modified with T-SC/SA. To be more specific, the doping of the organic semiconductor disappeared when the transistor is stored in darkness. Therefore the influence of light on devices made from P3HT, which contain an interface modification of T-SC/SA, has also been investigated.

The transfer characteristics in fig. 7.5 show that the threshold voltage of the transistor H_79 1L shifts from 39 V to -11 V when the device is stored for 21 hours in the dark (see tab. 7.3).

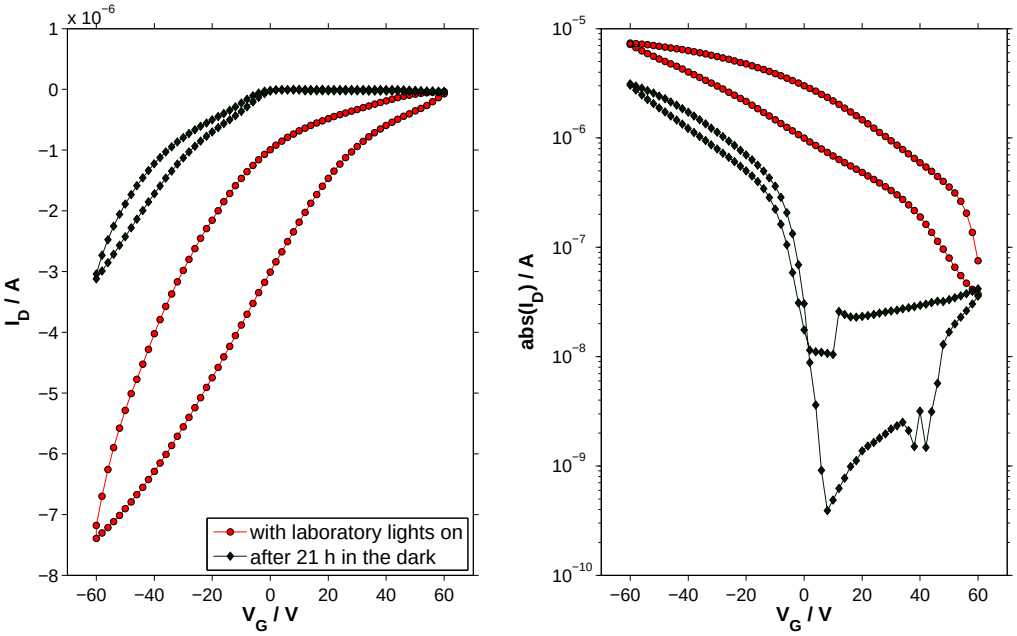

Figure 7.5: Transfer characteristics of an P3HT-OTFT modified with T-SC/SA measured with lights on and after 21 hours in the dark, $V_D = -10$ V;
OTFT nr. H_79 1L.

The cause of this behaviour could be the dependence of the acidity of a material on light exposure. This effect is called excited state proton transfer (ESPT) and was first published by Förster in 1950 [30]. It accounts for the fact that an acid molecule is promoted into an excited state by illumination and, thus, can be more acidic. For further information see the review on ESPT from Noam Agmon [31].

Nevertheless, it has to be pointed out that V_T is only several volts below zero when measured in the dark. Compared to the results of sec. 5.1, where a reference device exhibited a threshold voltage that lies at about -33 V when measured in the dark, one has to state that the T-SC/SA layer somehow shows a passivating behaviour in darkness.

Table 7.3: Properties of device H_79 1L from fig. 7.5
V_D ... applied drain voltage, μ_{sat} ... effective charge carrier mobility (fitted in linear regime), $V_{T,sat}$ ... threshold voltage (fitted in linear regime)

measured	V_D / V	μ_{lin} / $10^{-3}cm^2/Vs$	$V_{T,lin}$ / V
in the light	-10	1.3	39
after 21 h in the dark	-10	1.1	-11

Another explanation for the threshold voltage shift could be that two rivalling effects almost compensate each other: the doping of the P3HT is in fact happening, which causes a positive threshold voltage shift, but the absence of light shifts V_T back towards negative values.

Another feature in fig. 7.5 is the significant change of the hysteresis that can be explained by the completely different stress that the transistor is exposed to during the two measurements. The transistor is operating throughout the whole measurement range, which covers 120 V, when the characteristics are recorded with the laboratory lights on. In contrast, the measurements in the dark only stresses the transistor by 60 V.

The threshold voltage shift that can be achieved by using T-SC/SA is very impressing but a drawback of this kind of interface modification is the time-consuming and extensive production of the T-SC/SA layer. A solution to this problem can be a polymer such as PSSA that offers the same functional groups (see sec. 4.4) in its molecular structure but can simply be spin coated under ambient conditions.

7.2 P3HT on PSSA

An interface modification of an OTFT based on P3HT is only possible with a polymer that is soluble in an orthogonal solvent. Since P3HT is soluble in chlorinated hydrocarbons and aromatic hydrocarbons, which both are relatively apolar, the polymer PSSA is the perfect candidate for such a system, because it can be dissolved in water. The degree of polarity of a material can also be related to its dielectric constant ε. The higher its value, the higher the polarity. Tab. 7.4 lists the dielectric constants of water and two commonly used solvents of P3HT, chloroform and toluene.

Table 7.4: Dielectric constants of solvents; taken from [32]

	water	*chloroform*	*toluene*
ε	78.54	4.806	2.379

PSSA has already been used by our group to successfully shift V_T of OTFTs based on pentacene. In fact, the threshold voltage can be tuned by changing the concentration of the solution and thus altering the thickness of the PSSA layer and the degree of doping in the organic semiconductor. This experiment has been carried out by Lukas Ladinig and its result is shown in fig. 7.6.

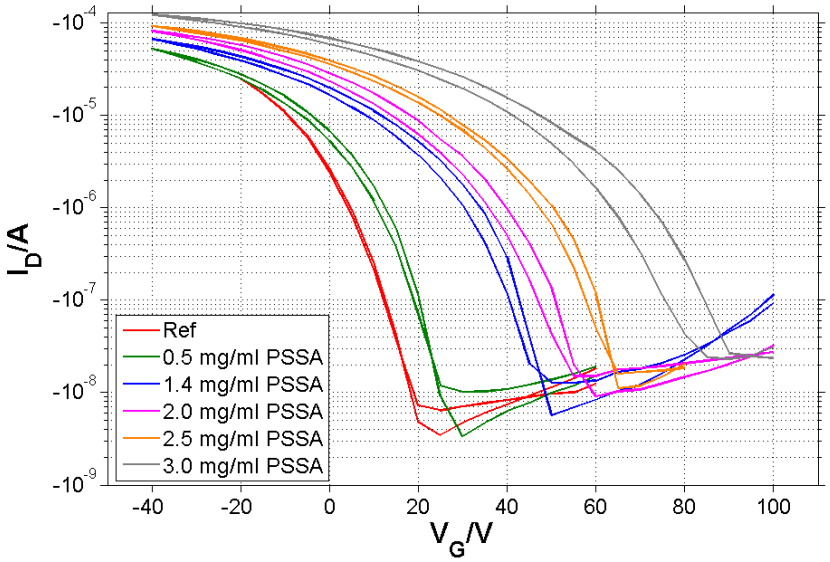

Figure 7.6: Transfer characteristics of OTFTs based on pentacene modified with PSSA made from different solution concentrations; measured by Lukas Ladinig

With little effort the threshold voltage is changed within a range of about 60 V. Unfortunately these results could not be reproduced by now.

Another promising finding was gained via Raman spectroscopy of a layer system that fits fig. 7.7 (without the gold electrodes).

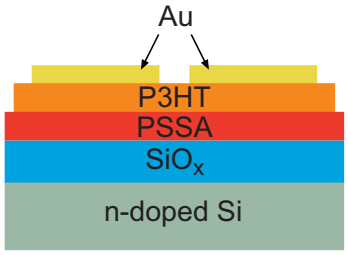

Figure 7.7: Layout of an OTFT with an additional layer made of PSSA.

Raman spectroscopy is used to record the oscillations that a molecule can perform and it is not restricted to oscillations that cause a change in the dipole moment of the molecule which is the case for infra-red spectroscopy.

Three different systems - P3HT, P3HT on T-SC/SA and P3HT on PSSA - have been analysed by Karin Pressl and Mauricio Musso at the University of Salzburg. The data that was retrieved is fitted with Lorentz fits (see fig. 7.8) and and three different modes can be determined at 1444 cm^{-1}, 1422 cm^{-1} and 1378 cm^{-1}. The two modes at 1444 cm^{-1} and 1378 cm^{-1} occur in every sample but the mode at 1422 cm^{-1} is only existent if the P3HT is doped. The amount of doping or at least a tendency can be gained by the shoulder at 1422 cm^{-1} in the spectrogram. Simulations have confirmed the experimental findings.

The well pronounced feature of the P3HT/PSSA system in fig. 7.8 is a very promising indication that this interface modification will cause a threshold voltage shift in an OTFT.

Unfortunately, there is an issue with the reproducibility of the results of the Raman spectroscopy. It has to be mentioned that these measurements have been performed three times and the corresponding shoulder at 1422 cm^{-1} was found twice.

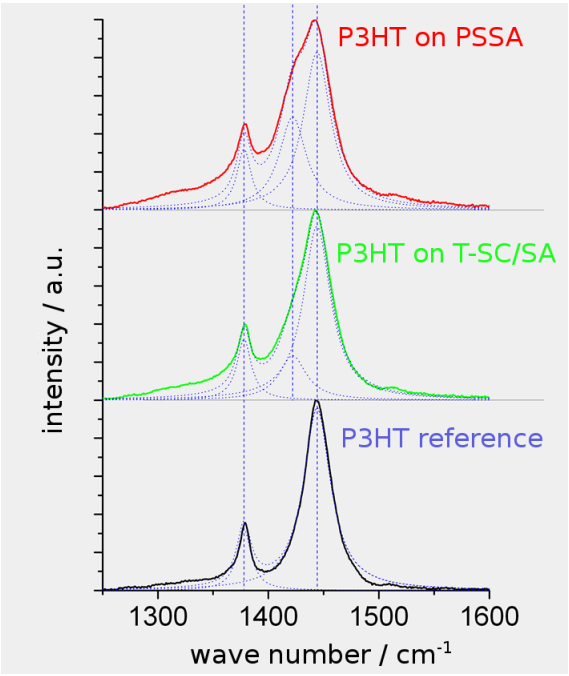

Figure 7.8: Raman spectroscopy of P3HT, P3HT on T-SC/SA and P3HT on PSSA; measurements and also evaluation were done by Karin Pressl and Maurizio Musso at the University of Salzburg;

The first PSSA-modified OTFTs contained a PSSA layer that was spin coated from a solution with a concentration of 2.5 mg/ml and the layer was heated at 80°C for 30 min in vacuum in order to dry it and get rid of residual water.

The results of such a modified transistor were rather disappointing (see fig. 7.9 and tab. 7.5). The most prominent feature in the transfer curves is the missing shift of the threshold voltage. In addition to that, the device exhibits a quite large hysteresis both in the transfer and the output characteristic. This might be an indication that there is still residual water present in the PSSA layer that messes with the organic semiconductor.

A comparison to a reference device reveals more interesting properties of the modified transistor. As one can see in fig. 7.10 the current in PSSA containing devices increases sub-linearly. This feature is caused by the so-called mobility degradation where the mobility decreases with the gate voltage. The reason for this effect are defects in the vicinity of the interface, for example charged centers, surface phonons or interface roughness [33].

The fact that interface roughness can cause mobility degradation is very interest-

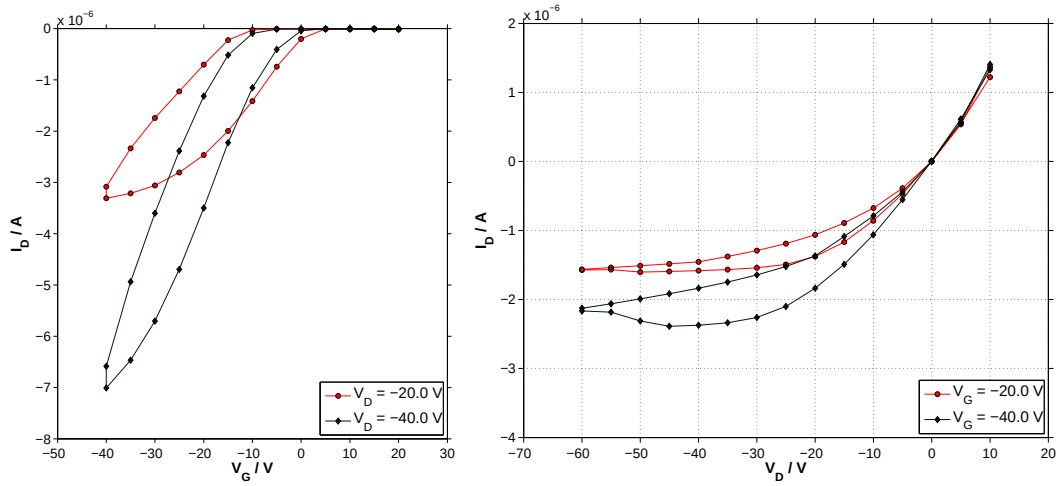

(a) Transfer characteristic (b) Output characteristic

Figure 7.9: Characteristics of an OTFT modified with PSSA 2.5 mg/ml, 80°C / 30 min; P3HT dissolved in chloroform;
OTFT nr. H_30 1R.

Table 7.5: Properties of device H_30 1R from fig. 7.9(a)
V_D ... applied drain voltage, μ_{sat} ... effective charge carrier mobility (fitted in saturation regime), $V_{T,sat}$ ... threshold voltage (fitted in saturation regime)

V_D / V	μ_{sat} / 10^{-3}cm^2/Vs	$V_{T,sat}$ / V
-20	1.7	6
-40	2.2	3

ing when one keeps in mind that the charge transport takes place near the interface at high gate voltages [7]. This can be an indication that the deposition of P3HT dissolves the PSSA layer at its surface, although they are soluble in orthogonal solvents.

Table 7.6: Properties of device H_28 2L and H_30 1R from fig. 7.10
V_D ... applied drain voltage, μ_{sat} ... effective charge carrier mobility (fitted in saturation regime), $V_{T,sat}$ ... threshold voltage (fitted in saturation regime)

device	V_D / V	μ_{sat} / 10^{-3}cm^2/Vs	$V_{T,sat}$ / V
reference	-40	2.1	11
P3HT on PSSA	-40	2.2	3

The bigger hysteresis at the higher gate voltage in the output characteristic in fig. 7.9(b) is a property that backs up this assumption.

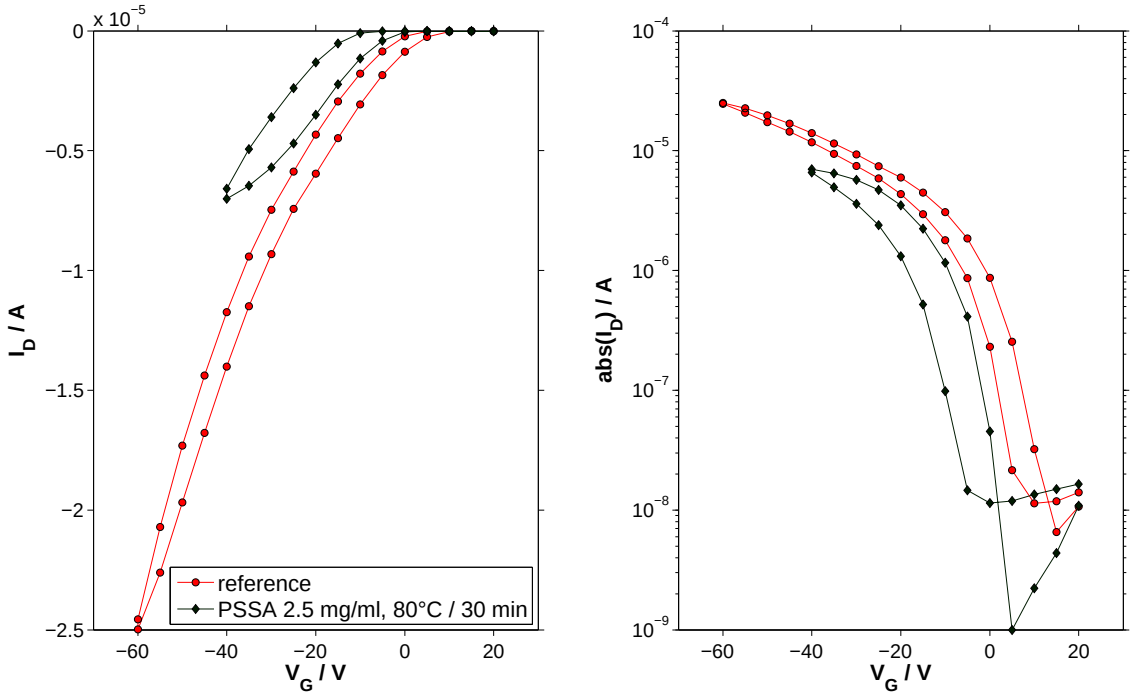

Figure 7.10: Comparison of transfer characteristics of a reference and a PSSA-modified device at $V_D = -40$ V;
OTFT nr. H_28 2L (reference) and H_30 1R (PSSA).

In order to minimize the influence of possible residual water in the devices, OTFTs with PSSA have been built which contained a PSSA layer that was heated at 110°C for 30 min to promote the drying process and the evaporation of water.

However, the characteristics of the devices showed no improvement (see fig. 7.11 and tab. 7.7).

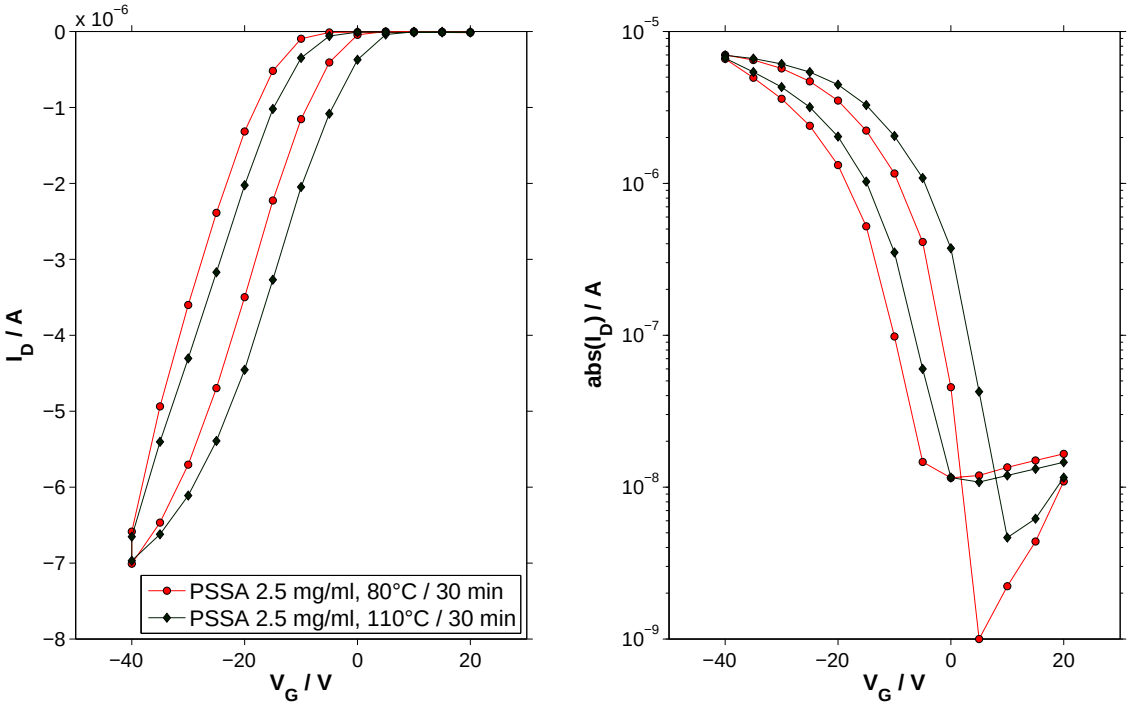

Figure 7.11: Comparison of transfer characteristics of two PSSA-modified devices heated at different temperatures measured at $V_D = -40$ V;
OTFT nr. H_30 1R (80°C) and H_32 1L (110°C).

Table 7.7: Properties of device H_30 1R and H_32 1R from fig. 7.11
V_D ... applied drain voltage, μ_{sat} ... effective charge carrier mobility (fitted in saturation regime), $V_{T,sat}$ ... threshold voltage (fitted in saturation regime)

PSSA heated at	V_D / V	μ_{sat} / 10^{-3}cm^2/Vs	$V_{T,sat}$ / V
80°C	-40	2.17	2.5
110°C	-40	2.01	7.5

7.3 Conclusion

The idea of shifting the threshold voltage with acidic materials works well with T-SC/SA, which has already been investigated by our group in recent years. It is no problem to reproduce former results with the new delivered P3HT and conduct new experiments.

On the other hand, the promising polymer PSSA does not provide the desired results. Although it has been shown by Lukas Ladinig that PSSA dopes the pentacene and there are certain experiments that hint towards a doping also of P3HT, the intended threshold voltage shift does not occur in OTFTs with P3HT on PSSA. One idea to explain this conflicting findings can be the formation of immobile charges due to the fact that the acidic residue, which is negatively charged, is strong enough to trap the generated charge carriers in its vicinity.

Furthermore, the analysis of the data implies that the two polymers P3HT and PSSA might intermix at the interface, even though their complementary solubility is supposed to prevent them from doing so.

As a result, the P3HT/PSSA system has been explored in more detail. The evaluation of these studies is included in the following chapter.

Chapter 8

Intermixing of orthogonally soluble polymers

The electronic examination of OTFTs with P3HT on PSSA is not sufficient to understand its behaviour. Therefore, additional x-ray measurements have been performed and evaluated by Alfred Neuhold to get a better insight into the P3HT/PSSA system. The three investigation techniques described in chapter 3 are used to gain information about the morphology of the polymer layers especially the interface roughness between the two polymers, the surface roughness of the organic semiconductor, and the orientation of its polymer chains.

As already discussed, the interface roughness plays an important role as far as the mobility degradation is concerned. The surface roughness might influence the charge carrier injection and the orientation of the polymer chains is crucial to the charge carrier mobility. Sirringhaus et al. [28] found out that the mobility increases in devices where the P3HT aligns edge-on on the substrate compared to a face-on alignment. This is because the interchain charge carrier transport mainly occurs via the overlapping π-orbitals of the polytiophene backbones.

The XRR measurement data which are acquired when analysing a system of two stacked thin-films, is a superposition of the responses of each layer. It is difficult to fit the data, if the layer thickness of the thin-films is similar. For this reason, the concentration of the PSSA and P3HT solution had to be changed.

As an additional parameter in this study, we also varied the solvent of P3HT and compared the results for chloroform (used for all devices discussed so far) with those of the even less polar solvent toluene.

In addition to the PSSA another water soluble acidic polymer has been used to investigate the intermixing. This polymer is poly acrylic acid (PAA) which is also intended to dope the organic semiconductor and thus shift the threshold voltage (see sec. 4.4).

8.1 P3HT on PSSA

The first system that is discussed in detail is the P3HT-PSSA layout that has already been dealt with in the previous chapter. In order to achieve a layer system that complies with the requirements mentioned above, the concentration of the P3HT and PSSA solutions had to be changed. The adjusted solution concentration and the corresponding layer thickness are listed in tab. 8.1.

Table 8.1: Solution concentrations c and layer thickness d that are used for the investigation of intermixing with PSSA;

solution	c / mg/ml	d / nm
PSSA/water	3.6	8
P3HT/chloroform	6	40
P3HT/toluene	10	40

The investigations focus on the influence of two parameters: the organic semiconductor's solvent and the treatment of the PSSA layer, where one has to distinguish between not heated samples and films heated at 80°C in vacuum for two hours before P3HT deposition.

8.1.1 P3HT/chloroform on PSSA

At first the system with P3HT processed from a solution of chloroform on a PSSA layer is discussed:

Structural analysis

The alignment of the P3HT chains was investigated by XRD and GIXD measurements and it was found that the polymer chains arrange in a face-on configuration (see fig. 8.1(a)) regardless of the subjacent layer. There is no difference, whether the PSSA layer was heated or not. Only when P3HT is deposited on silicon oxide

the alignment of the P3HT chains is not strictly parallel to the dielectric substrate but it is a little bit tilted (see fig. 8.1(b)).

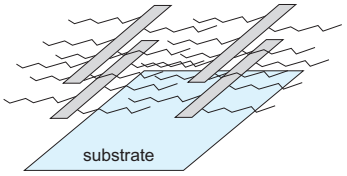

(a) P3HT/$CHCl_3$ on PSSA: face-on, parallel to dielectric substrate

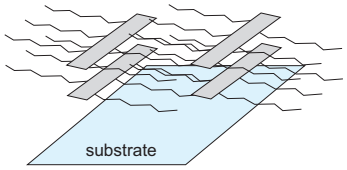

(b) P3HT/$CHCl_3$ on SiO_x: face-on, slightly tilted

Figure 8.1: Alignment of P3HT polymer chains when deposited from a chloroform solution

The next issues concerning the morphology of the P3HT layer are the interface and surface roughness which have been investigated by XRR measurements.

The roughness of a PSSA layer (whether heated or unheated) prior to the deposition of P3HT is only 0.4 nm which is of the same range as the one of the subjacent SiO_x substrate. After the spin coating of P3HT it is several times bigger than before (see tab. 8.2). The interface roughness of the unheated PSSA layer is 2.5 nm which is almost twice as many as the one of the heated PSSA layer. It is now evident that the P3HT/$CHCl_3$ solution dissolves the PSSA layer at the surface but the impact can be reduced by annealing the PSSA layer.

Table 8.2: Interface (σ_I) and surface roughness (σ_S) and alignment of the P3HT polymer chains processed from a chloroform solution;

layout	σ_I / nm	σ_S / nm	alignment
P3HT on SiO_x	0.5	1.4	face-on (slightly tilted)
P3HT on PSSA n.v.h.	2.5	0.7	face-on
P3HT on PSSA v.h. at 80°C	1.3	0.8	face-on

In contrast to the interface roughness, the surface roughness of P3HT decreases, when it is deposited on a PSSA layer, compared to P3HT on silicon oxide. The improved parallel alignment of the polymer chains could be a reason for this effect.

Device characterization

Besides the structural analysis it is of interest what the performance of the OTFTs is like. A representative selection of the three possible configurations - P3HT on

silicon oxide, P3HT on a not heated PSSA layer and P3HT on a heated PSSA layer - is displayed in comparison. The results are shown in fig. 8.2 and tab. 8.3. The

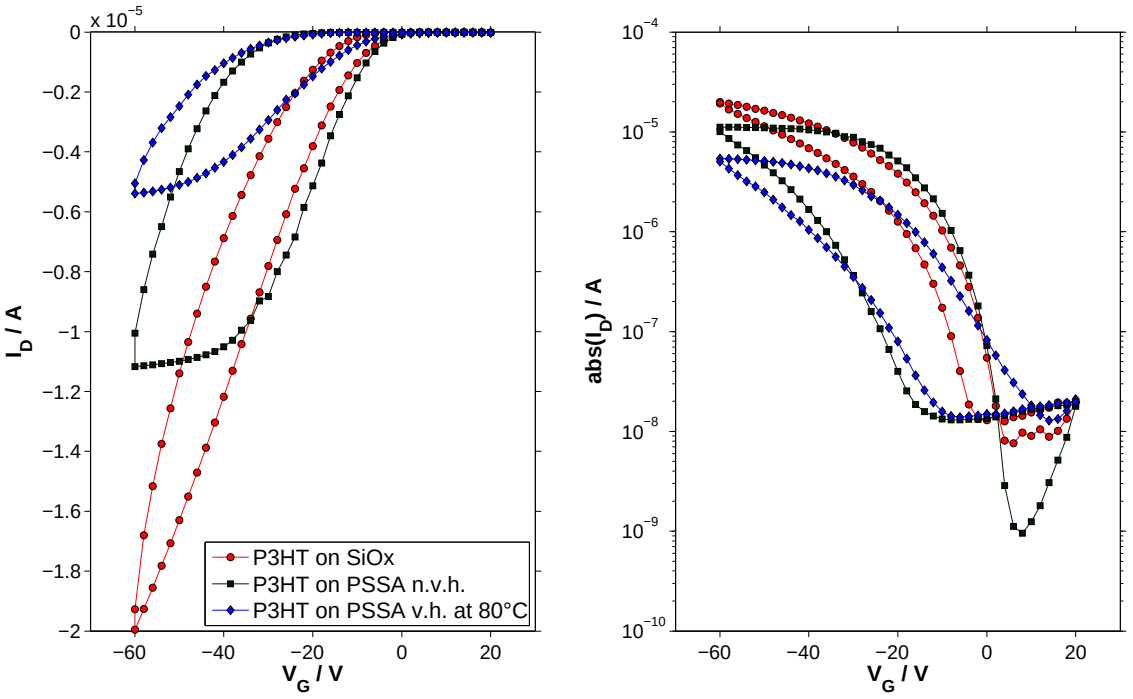

Figure 8.2: Comparison of transfer characteristics of an SiO_x, a not vacuum-heated (n.v.h.) PSSA and a vacuum-heated (v.h.) PSSA device with P3HT/$CHCl_3$; V_D = -40 V;
OTFT nr. H_116 1R (reference), H_119 1R (PSSA n.v.h.) and H_120 1R (PSSA v.h.).

Table 8.3: Properties of device H_116 1R, H_119 1R and H_120 1R from fig. 8.2
V_D ... applied drain voltage, μ_{sat} ... effective charge carrier mobility (fitted in saturation regime), $V_{T,sat}$ ... threshold voltage (fitted in saturation regime)

device	V_D / V	μ_{sat} / $10^{-3}cm^2/Vs$	$V_{T,sat}$ / V
SiO_x	-40	2.60	0.9
PSSA n.v.h.	-40	3.38	1.6
PSSA v.h. at 80°C	-40	0.91	2.0

first obvious feature is the bigger hysteresis that occurs in devices with a PSSA layer regardless of its preparation. It was already stated in sec. 7.2 that residual water might cause this effect. A more interesting aspect is the large difference in the mobility of the two PSSA-modified OTFTs. The strongly decreased mobility in transistors with a heated PSSA layer does not agree with the results in sec. 7.2.

But it has to be stated that there was only one wafer available because the back-up sample became useless due to a mishap during the gold evaporation which resulted in a conducting channel across source and drain in all of the four transistors on the substrate.

Furthermore, the mobility degradation is not as big in the devices with the heated PSSA as it is in devices with unheated PSSA. This can be attributed to the difference in the interface roughness because the mobility degradation is sensitive to defects at the interface.

A short glimpse at the statistic of the transfer characteristics of OTFTs that have the device structure at hand is shown in fig. 8.3 and tab. 8.4. The performance of the P3HT on SiO_x and P3HT on heated PSSA devices vary significantly, even on a single substrate, but the P3HT on unheated PSSA devices show a fairly regular behaviour, even on two different substrates.

Table 8.4: Evaluation of the statistic from fig. 8.3 using average and standard deviation;
V_D ... applied drain voltage, μ_{sat} ... effective charge carrier mobility (fitted in saturation regime), $V_{T,sat}$ ... threshold voltage (fitted in saturation regime)

device	V_D / V	μ_{sat} / $10^{-3}cm^2/Vs$	$V_{T,sat}$ / V
SiO_x	-40	3 ± 2	2 ± 4
PSSA n.v.h.	-40	3.3 ± 0.5	1 ± 3
PSSA v.h. at 80°C	-40	0.6 ± 0.3	5 ± 5

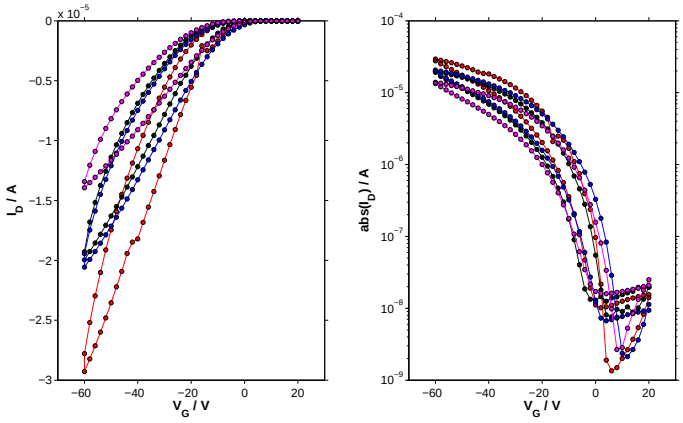

(a) P3HT/$CHCl_3$ on SiO_x

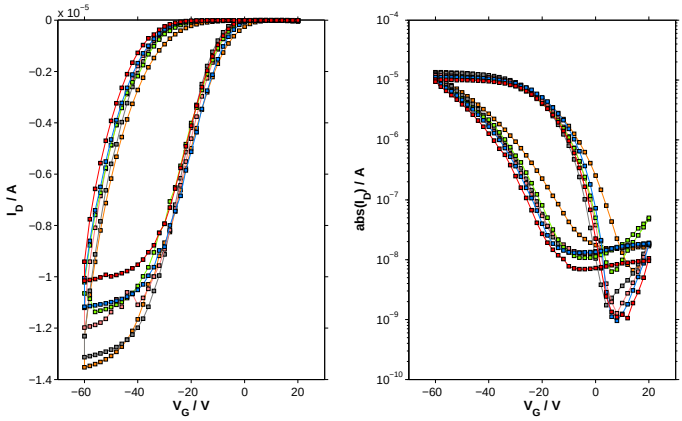

(b) P3HT/$CHCl_3$ on PSSA n.v.h.

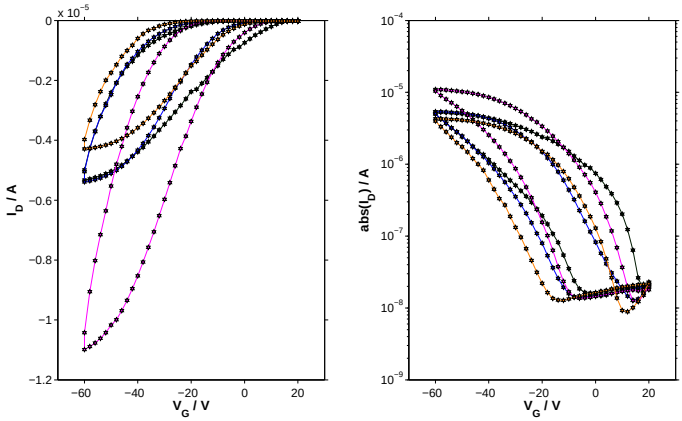

(c) P3HT/$CHCl_3$ on PSSA v.h.

Figure 8.3: Statistic of transfer characteristics of SiO_x (circle), not vacuum-heated PSSA (rectangle) and vacuum-heated PSSA (star) devices with P3HT/$CHCl_3$; V_D = -40 V;

8.1.2 P3HT/toluene on PSSA

With toluene as the new solvent it was assumed that the overall performance of the transistors should improve, since Chang et al. [27] have shown that solutions made from high-boiling point solvents promote the self-organisation of the polymer chains (boiling point of chloroform = 61°C; boiling point of toluene = 111°C). But at first, the morphology of the layer system will be discussed.

Structural analysis

The results of the XRD and GIXD analysis show indeed that the P3HT chains align in edge-on configuration, if the organic semiconductor is dissolved in toluene, which corresponds to the findings of Chang et al. [27]. However, the alignment of the polymer chains is tilted again in the devices with P3HT on SiO_x (see fig. 8.4).

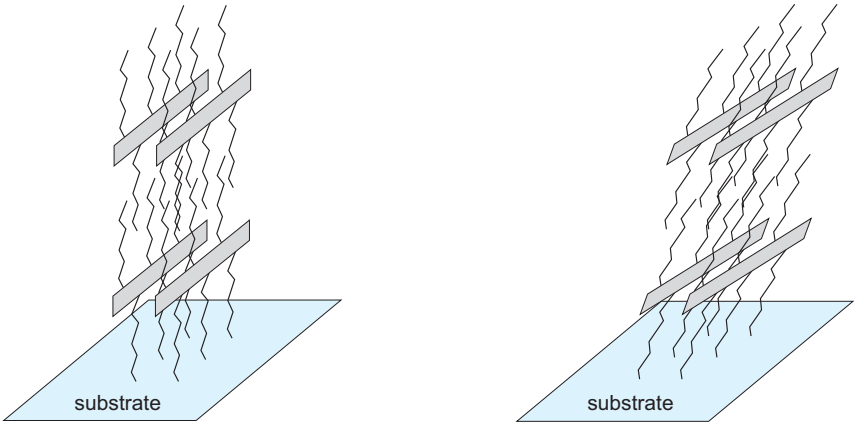

(a) P3HT/toluene on PSSA: edge-on, perpendicular to dielectric substrate

(b) P3HT/toluene on SiO_x: edge-on, slightly tilted

Figure 8.4: Alignment of P3HT polymer chains when deposited from a toluene solution

XRR measurements revealed that the interface roughness is now independent of the treatment of the PSSA layers and still as small (0.4 nm) as before the P3HT deposition (see tab. 8.5). On the other hand, the surface roughness of P3HT is significantly higher when it is processed from a toluene solution (4.7 to 6.1 nm compared to 0.7 to 1.4 nm of P3HT/$CHCl_3$ layers). The rough P3HT surface can be caused by the edge-on alignment that provides different grain sizes than a face-on ordering.

Table 8.5: Interface (σ_I) and surface roughness (σ_S) and alignment of the P3HT polymer chains processed from a toluene solution;

layout	σ_I / nm	σ_S / nm	alignment
P3HT on SiO_x	0.5	4.9	edge-on (slightly tilted)
P3HT on PSSA n.v.h.	0.4	6.1	edge-on
P3HT on PSSA v.h. at 80°C	0.4	4.7	edge-on

Device characterization

Fig. 8.5 and tab. 8.6 show the results of the OTFT characterization. The mobility in the P3HT on SiO_x device has doubled and the PSSA-modified transistors exhibit a mobility that is one order of magnitude higher than in OTFTs made from P3HT/$CHCl_3$. This can be attributed to the preferable edge-on alignment of P3HT chains when deposited from a toluene solution. Due to the new morphology and the rough P3HT surface (locally higher electric field) the charge carrier injection from the gold electrodes into the organic semiconductor could have improved, which would also contribute to a better effective charge carrier mobility.

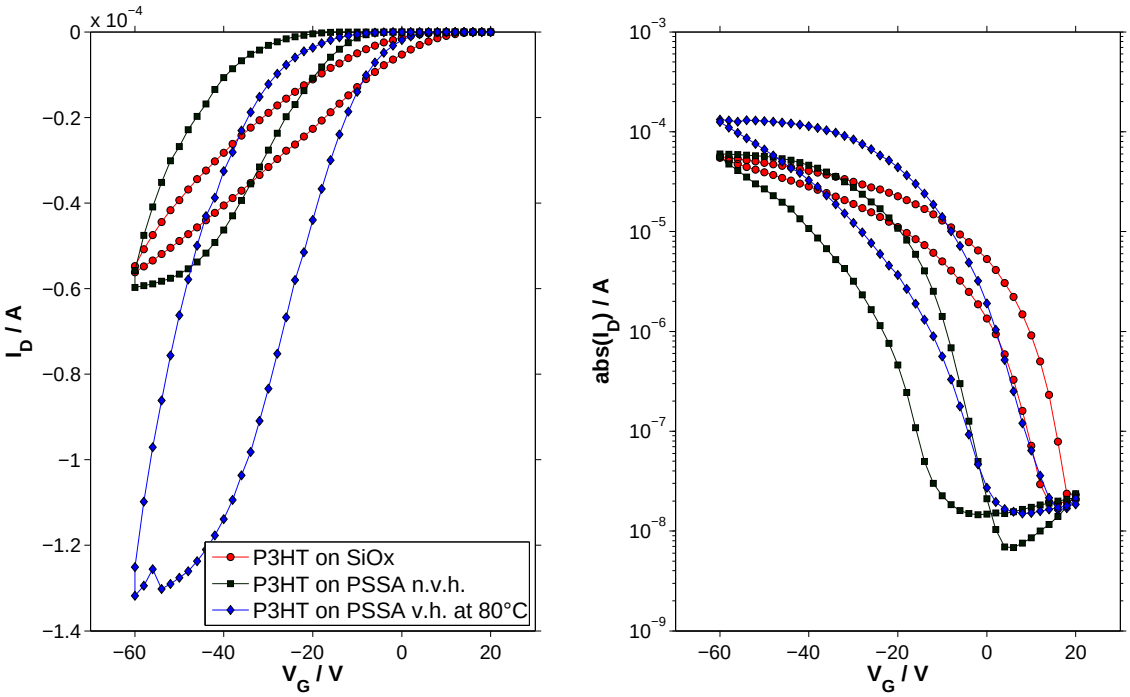

Figure 8.5: Comparison of the transfer characteristics of an SiO_x, a not vacuum-heated PSSA and a vacuum-heated PSSA device with P3HT/toluene; V_D = -40 V; OTFT nr. H_123 1R (SiO_x), H_124 1R (PSSA n.v.h.) and H_126 1R (PSSA v.h.).

Nevertheless, the hysteresis is as big as before and mobility degradation is still present although it is reduced. The smooth PSSA/P3HT interface and the new orientation of the polymer chains seem to reduce the amount of defects in the vicinity of the interface.

Table 8.6: Properties of device H_123 1R, H_124 1R and H_126 1R from fig. 8.5; V_D ... applied drain voltage, μ_{sat} ... effective charge carrier mobility (fitted in saturation regime), $V_{T,sat}$ ... threshold voltage (fitted in saturation regime)

device	V_D / V	μ_{sat} / $10^{-3}cm^2/Vs$	$V_{T,sat}$ / V
SiO_x	-40	5.3	17
PSSA n.v.h.	-40	13	-4.5
PSSA v.h. at 80°C	-40	25	3.0

However, the statistic of this system in fig. 8.7 and tab. 8.7 shows that the performance varies in the same range in all layer systems.

Wrapping up the results of the investigations on PSSA-P3HT devices one can say that the intermixing only takes place if the P3HT solution is made from chloroform but the surface roughness increases if the P3HT is processed from a toluene solution (see fig.8.6). This means that it is of importance to choose the right solvents in a stacked polymer layout even if they are orthogonally soluble.

(a) P3HT/$CHCl_3$ on PSSA

(b) P3HT/toluene on PSSA

Figure 8.6: Schematic drawing of interface and surface roughness of PSSA-P3HT layer systems;

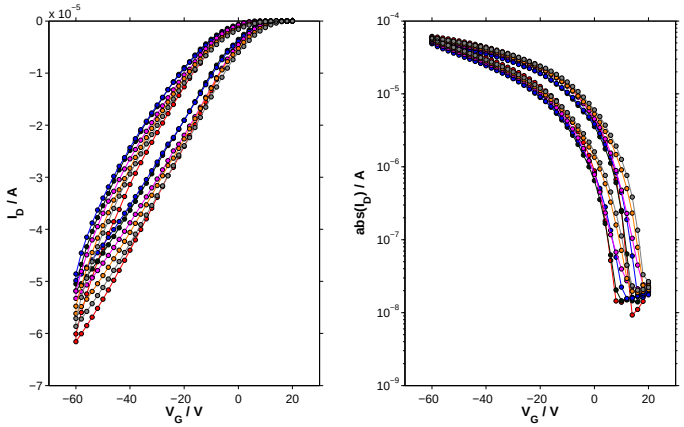

(a) P3HT/toluene on SiO_x

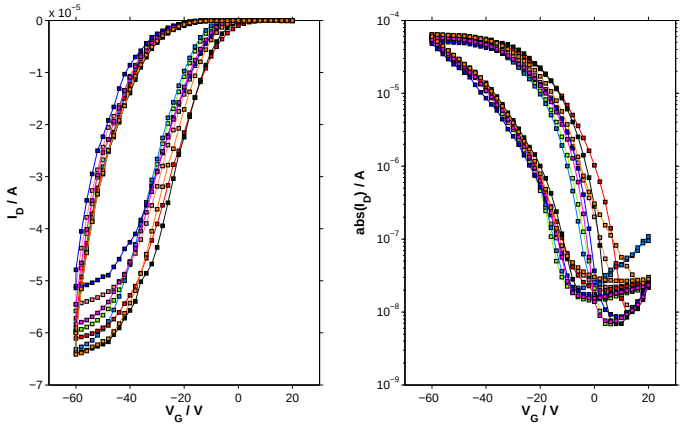

(b) P3HT/toluene on PSSA n.v.h.

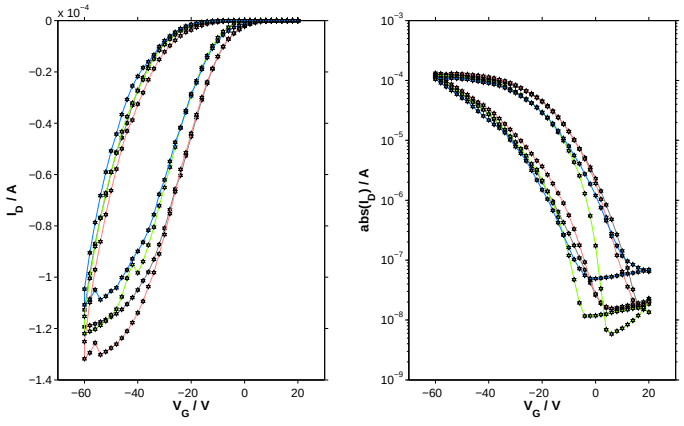

(c) P3HT/toluene on PSSA v.h.

Figure 8.7: Statistic of transfer characteristics of SiO_x (circle), not vacuum-heated PSSA (rectangle) and vacuum-heated PSSA (star) devices with P3HT/toluene; V_D = -40 V;

Table 8.7: Evaluation of the statistic from fig. 8.7 using average and standard deviation;
V_D ... applied drain voltage, μ_{sat} ... effective charge carrier mobility (fitted in saturation regime), $V_{T,sat}$ ... threshold voltage (fitted in saturation regime)

device	V_D / V	μ_{sat} / $10^{-3}cm^2/Vs$	$V_{T,sat}$ / V
SiO_x	-40	5.9 ± 0.9	15 ± 2
PSSA n.v.h.	-40	13 ± 1	-2 ± 3
PSSA v.h. at 80°C	-40	24 ± 2	1 ± 2

8.2 P3HT on PAA

The second water soluble polymer, PAA, which is used to investigate the interdiffusion of polymers, is handled in the same way as PSSA. The layer fabrication is described in sec. 4.4 and is overall not different from the PSSA layer fabrication. The functional group of PAA is not the same but similar to the one of PSSA and, thus, also intended to induce a threshold voltage shift. In fact, measurements with PAA-modified OTFTs based on pentacene have already been conducted by Lukas Ladinig and a threshold voltage shift was observed.

The layer thickness of PAA and its corresponding solution concentration was changed after the measurements for the chloroform related part were finished. The according details are listed in tab. 8.8. The concentration of the P3HT solutions has not been changed for these experiments performed in this chapter.

Table 8.8: Solution concentrations c and layer thickness d that are used for the investigation of interdiffusion with PAA;

solution	c / mg/ml	d / nm
P3HT/chloroform	6	40
P3HT/toluene	10	40
chloroform: PAA/water	4.4	7
toluene: PAA/water	5	9

To start with, the transistors that have been built for the investigation of the PAA-P3HT systems, exhibit a significantly smaller effective charge carrier mobility than the ones of the PSSA-P3HT systems. As already stated in sec. 5.1, it happened a few times, that the mobility was in the range of $10^{-4}cm^2/Vs$. However, it is a strange coincidence that this is the case for all investigations concerning PAA. The

solutions have been used within one day after their production and there has only been used one P3HT/chloroform and one P3HT/toluene solution for all samples, included the x-ray samples. Therefore the results within one examined system are valid.

8.2.1 P3HT/chloroform on PAA

At first, the P3HT/chloroform on PAA system is discussed, starting with the structural analysis of the P3HT layer.

Structural analysis

The evaluation of the XRD and GIXD measurement data show that the P3HT aligns face-on on a PAA layer and the polymer chains posses a better parallel alignment relative to the dielectric substrate compared to P3HT/chloroform on SiO_x (see fig. 8.8).

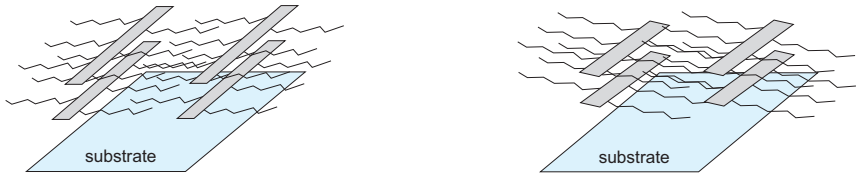

(a) P3HT/$CHCl_3$ on PAA: face-on, parallel to dielectric substrate

(b) P3HT/$CHCl_3$ on SiO_x: face-on, slightly tilted

Figure 8.8: Alignment of P3HT polymer chains when deposited from a chloroform solution

The overview of the morphological properties in tab. 8.9 reveals that the interface roughness is low, no matter whether the PAA layer has been heated or not. Since the surface roughness of the PAA layer is 0.3 nm (unheated) and 0.4 (heated) before the P3HT deposition, it can be a sign that hardly any dissolving occurs. In fact, the XRR measurements deliver different results depending on the region where the beam hits the wafer and this discrepancies are in the same range as the difference between PAA before and after the spin coating of P3HT. The surface roughness of P3HT is slightly reduced, when it is spun on a PAA layer.

Comparing the results of the structural analysis of the P3HT/chloroform on PAA system to the ones of the P3HT/chloroform on PSSA system, one can say that PAA

Table 8.9: PAA: interface (σ_I) and surface roughness (σ_S) and alignment of the P3HT polymer chains processed from a chloroform solution;

layout	σ_I / nm	σ_S / nm	alignment
P3HT on SiO_x	0.5	1.4	face-on (slightly tilted)
P3HT on PAA n.v.h.	0.5	0.9	face-on
P3HT on PAA v.h. at 80°C	0.4	1.0	face-on

is not as sensitive to orthogonal solvents as PSSA. Nevertheless, the alignment and the surface roughness of P3HT is the same.

Device characterization

The device characteristics in fig. 8.9 and the fitted parameters in tab. 8.10 show that there is virtually no difference whether the PAA was heated or not. This is consistent with to the findings that have been gained via x-ray analysis.

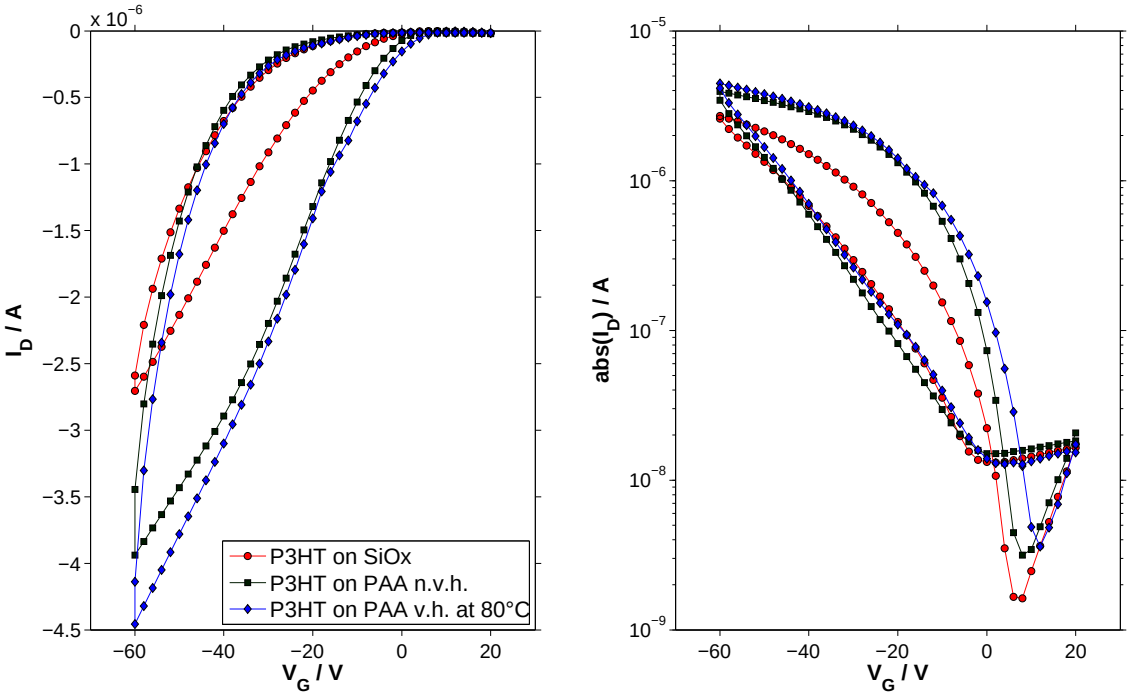

Figure 8.9: Comparison of transfer characteristics of an SiO_x, a not vacuum-heated PAA and a vacuum-heated PAA device with P3HT/$CHCl_3$; V_D = -40 V;
OTFT nr. H_147 1L (SiO_x), H_148 2L (PAA n.v.h.) and H_150 1L (PAA v.h.).

An interesting aspect is that the performance of the PAA-modified transistor exceeds the one of the reference device. The PAA layer might offers a surface to

the P3HT that boosts the alignment of P3HT resulting in bigger grain sizes and thus reducing the grain boundaries that limit the charge transport. Another feature is the less pronounced mobility degradation at high gate voltages compared to the P3HT/chloroform on PSSA system, which may result from fewer defects near the vicinity of the interface. Nevertheless, the hysteresis is very big, which is again most likely caused by residual water from the PAA-solution.

Table 8.10: Properties of device H_147 1L, H_148 2L and H_150 1L from fig. 8.9; V_D ... applied drain voltage, μ_{sat} ... effective charge carrier mobility (fitted in saturation regime), $V_{T,sat}$ ... threshold voltage (fitted in saturation regime)

device	V_D / V	μ_{sat} / $10^{-4}cm^2/Vs$	$V_{T,sat}$ / V
SiO_x	-40	2.4	3.4
PAA n.v.h.	-40	6.3	5.9
PAA v.h. at 80°C	-40	5.5	9.2

The statistic in fig. 8.10 and tab. 8.11 reveal that the fluctuation of the data is significantly reduced compared to the one of 'PSSA-P3HT' experiments.

The results of the statistical evaluation also show that there is a small shift to larger threshold voltages when the PAA layer is present, which is too small to speak of doping of the organic semiconductor.

Table 8.11: Evaluation from fig. 8.10 using average and standard deviation; V_D ... applied drain voltage, μ_{sat} ... effective charge carrier mobility (fitted in saturation regime), $V_{T,sat}$ ... threshold voltage (fitted in saturation regime)

device	V_D / V	μ_{sat} / $10^{-4}cm^2/Vs$	$V_{T,sat}$ / V
SiO_x	-40	2.5 ± 0.1	3 ± 2
PAA n.v.h.	-40	7 ± 1	8 ± 2
PAA v.h. at 80°C	-40	7 ± 1	8 ± 2

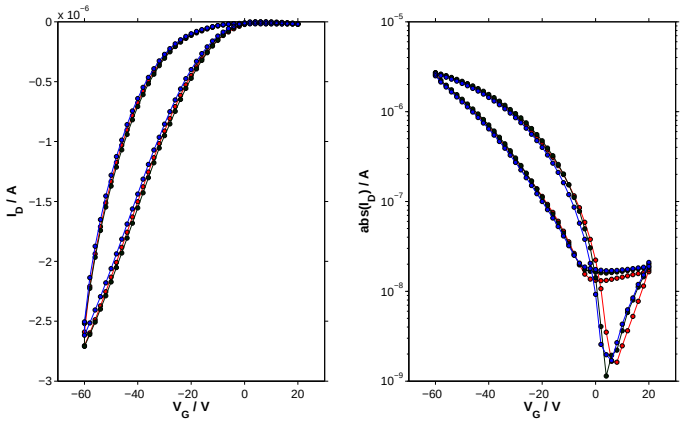

(a) P3HT/$CHCl_3$ on SiO_x

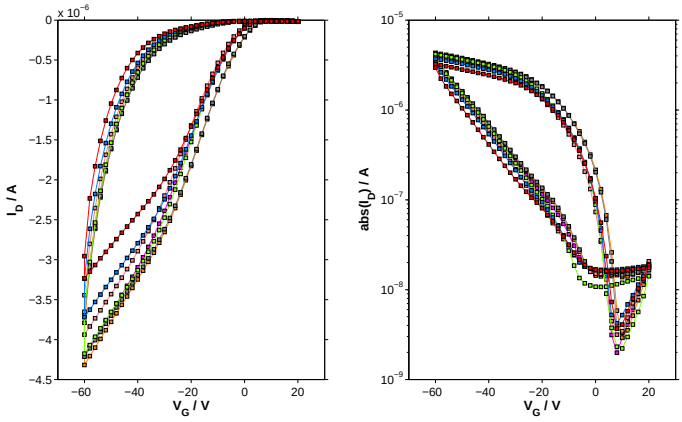

(b) P3HT/$CHCl_3$ on PAA n.v.h.

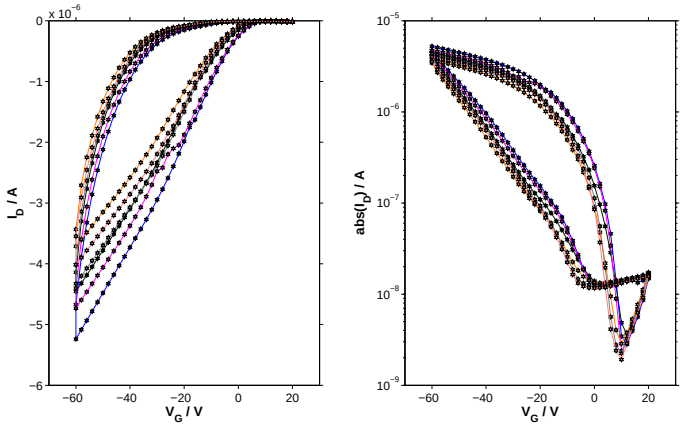

(c) P3HT/$CHCl_3$ on PAA v.h.

Figure 8.10: Statistic of transfer characteristics of SiO_x (circle), not vacuum-heated PAA (rectangle) and vacuum-heated PAA (star) devices with P3HT/$CHCl_3$; V_D = -40 V;

8.2.2 P3HT/toluene on PAA

At last the P3HT/toluene on PAA system is discussed, starting with the structural analysis.

Structural analysis

XRD and GIXD measurements show that the alignment of the organic semiconductor on a PAA layer is edge-on when the P3HT is processed from a toluene solution (see fig. 8.11). This result matches the one in the 'PSSA-P3HT/toluene' study.

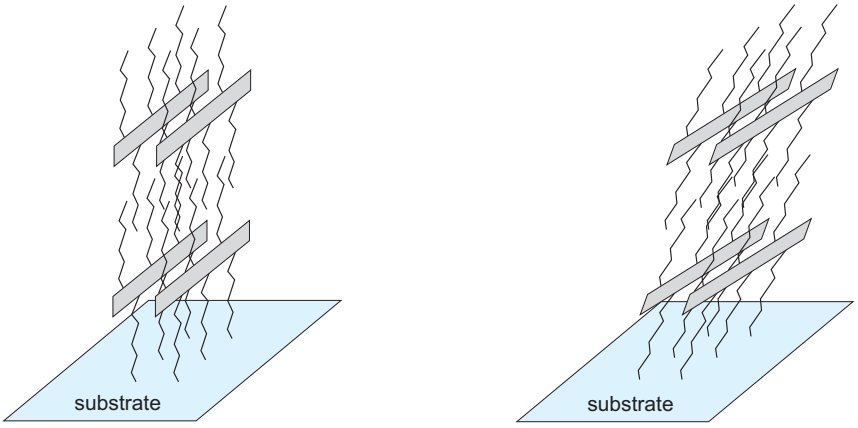

(a) P3HT/toluene on PAA: face-on, parallel to dielectric substrate

(b) P3HT/toluene on SiO_x: face-on, slightly tilted

Figure 8.11: Alignment of P3HT polymer chains when deposited from a toluene solution

The evaluation of the XRR measurements reveal that the surface roughness increases if the P3HT is processed from a toluene solution (see tab. 8.12). Additionally the interface is slightly smoother than the one of P3HT/chloroform on PAA.

Table 8.12: PAA: interface (σ_I) and surface roughness (σ_S) and alignment of the P3HT polymer chains processed from a toluene solution;

layout	σ_I / nm	σ_S / nm	alignment
P3HT on SiO_x	0.5	4.9	edge-on (slightly tilted)
P3HT on PAA n.v.h.	0.4	5.4	edge-on
P3HT on PAA v.h. at 80°C	0.2	4.6	edge-on

Overall, one can say that the structure of the P3HT layer is essentially the same in 'PAA-P3HT' and 'PSSA-P3HT' systems, when the organic semiconductor is deposited from a toluene solution.

Device characterization

A comparison of the transfer characteristics of an SiO_x, a not vacuum-heated PAA and a vacuum-heated PAA device with P3HT/toluene in fig. 8.12 and tab. 8.13 shows that the mobility and the threshold voltage of all three configurations is in the same range. There seems to be no influence of the treatment of the PAA layer on the transfer characteristics which is consistent to the results of the structural analysis. The bigger hysteresis in OTFTs with P3HT on PAA is again likely to be caused by residual water from the PAA-solution.

The mobility degradation seems to be somewhat bigger compared to the P3HT/chloroform on PAA system. Maybe the edge-on alignment is more sensitive to the present defects than the face-on alignment.

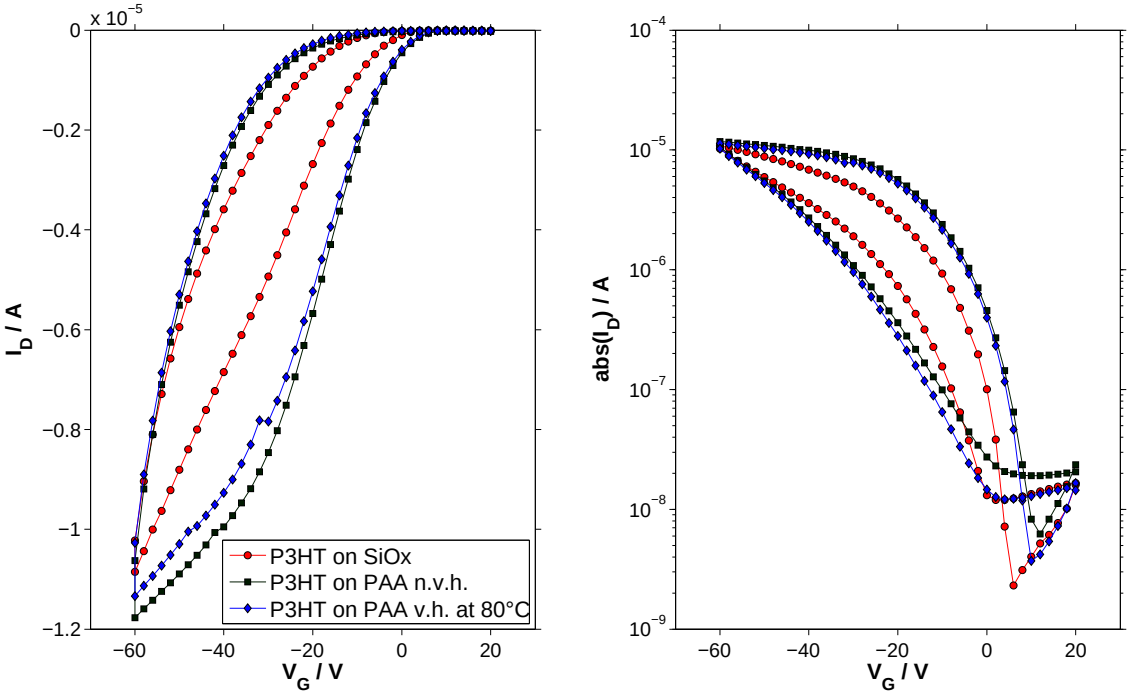

Figure 8.12: Comparison of transfer characteristics of an SiO_x, a not vacuum-heated PAA and a vacuum-heated PAA device with P3HT/toluene; V_D = -40 V;
OTFT nr. H_152 1R (SiO_x), H_153 1L (PAA n.v.h.) and H_156 2L (PAA v.h.).

Table 8.13: Properties of device H_152 1R, H_153 1L and H_156 2L from fig. 8.12; V_D ... applied drain voltage, μ_{sat} ... effective charge carrier mobility (fitted in saturation regime), $V_{T,sat}$ ... threshold voltage (fitted in saturation regime)

device	V_D / V	μ_{sat} / $10^{-3}cm^2/Vs$	$V_{T,sat}$ / V
SiO_x	-40	1.4	4.2
PAA n.v.h.	-40	2.3	7.5
PAA v.h. at 80°C	-40	2.2	7.1

The statistics in fig. 8.13 show that the characteristics are very stable and reproducible. The evaluation in tab. 8.14 also indicates that there is nearly no difference between heated and unheated PAA layers.

Table 8.14: Evaluation of statistic from fig. 8.13 using average and standard deviation;
V_D ... applied drain voltage, μ_{sat} ... effective charge carrier mobility (fitted in saturation regime), $V_{T,sat}$ ... threshold voltage (fitted in saturation regime)

device	V_D / V	μ_{sat} / $10^{-3}cm^2/Vs$	$V_{T,sat}$ / V
SiO_x	-40	1.3 ± 0.2	5 ± 2
PAA n.v.h.	-40	2.4 ± 0.3	7.7 ± 0.5
PAA v.h. at 80°C	-40	2.2 ± 0.2	7.8 ± 0.6

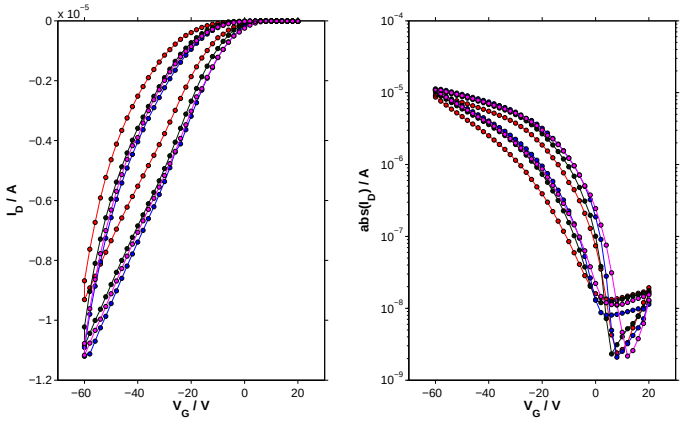

(a) P3HT/toluene on SiO_x

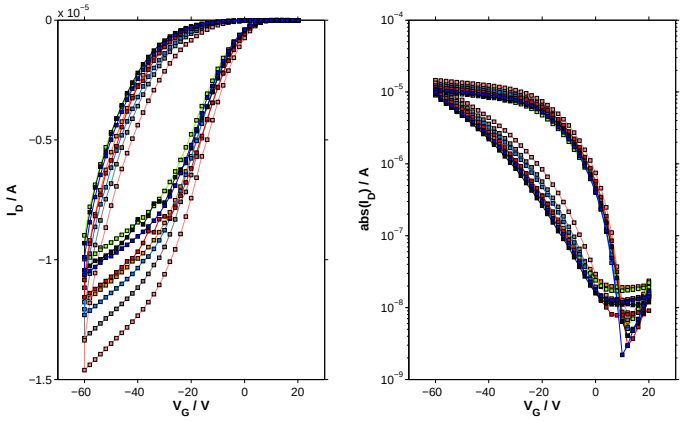

(b) P3HT/toluene on PAA n.v.h.

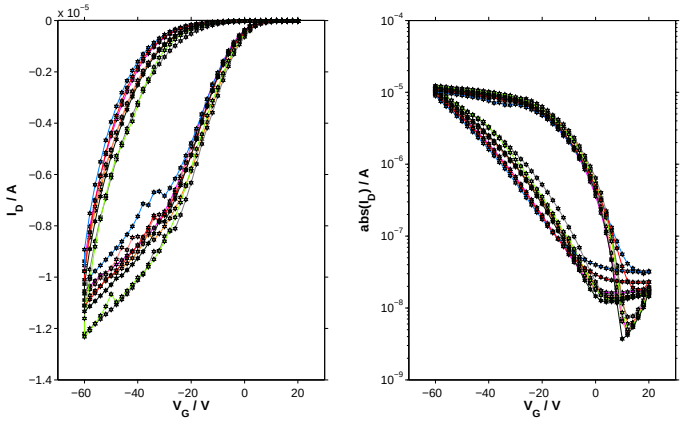

(c) P3HT/toluene on PAA v.h.

Figure 8.13: Statistic of transfer characteristics of SiO_x (circle), not vacuum-heated PAA (rectangle) and vacuum-heated PAA (star) devices with P3HT/toluene; V_D = -40 V;

8.3 Conclusion

Summing up the findings of this chapter one can conclude that it is possible to dissolve a polymer with another polymer that is solved in an orthogonal solvent but the degree of intermixing can be reduced by annealing the subjacent polymer layer and the choice of the solvent. Chloroform has more impact on a water soluble polymer than toluene, which is attributed to the difference in polarity.

Additionally, the polymer itself has a large influence on the intermixing process. The PAA polymer is less sensitive to orthogonal solvents - if at all - than the PSSA polymer.

Furthermore, the big difference between chloroform and toluene solutions is that chloroform forms a rough interface combined with a smooth surface and in contrast to that, toluene forms a smooth interface combined with a rough surface. Of course the alignment of the organic semiconductor is preferable in toluene based fabrication to the one of chloroform. The reason why toluene solutions of P3HT result in a rough surface is an issue of current research.

The interesting and new results of the study on intermixing of orthogonal soluble polymers are schematically shown in fig. 8.14.

However, because of the generally small mobilities of the PAA-P3HT devices the results definitely need to be confirmed before any other experiments can be conducted.

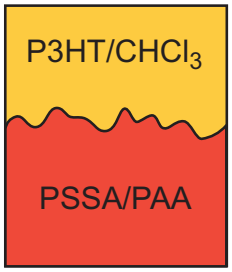

(a) Interface and surface roughness of P3HT/$CHCl_3$ on PSSA/PAA

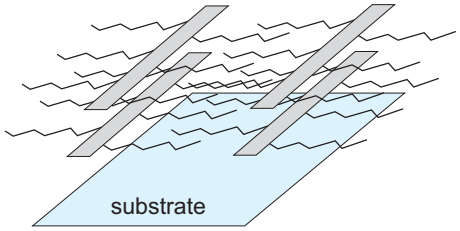

(b) Alignment of P3HT/$CHCl_3$ on PSSA/PAA

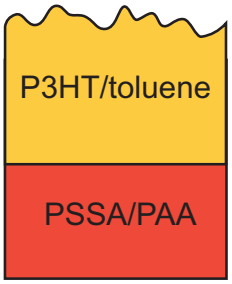

(c) Interface and surface roughness of P3HT/toluene on PSSA/PAA

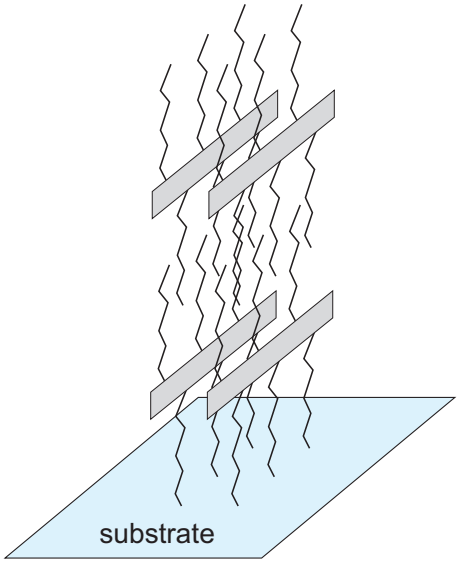

(d) Alignment of P3HT/toluene on PSSA/PAA

Figure 8.14: Interface and surface roughness and corresponding alignment of P3HT polymer chains when deposited from a chloroform or toluene solution;

Chapter 9

Summary

This thesis shows that OTFTs built from the P3HT purchased from Rieke Metals are working properly and that they deliver reasonably good results. The performance of the devices can be enhanced by putting a passivation layer on the silicon oxide substrate but, nevertheless, the transistors are very sensitive to bias stress.

The threshold voltage can easily be shifted by several ten volts with a layer of T-SC/SA, but the doping process which is responsible for the threshold voltage shift is strongly influenced by light.

On the other hand, the acidic water soluble polymer PSSA does not cause a threshold voltage shift, although this has been indicated by Raman scattering. This lead to further investigations, which confirmed the assumption, that the P3HT solution is dissolving the subjacent PSSA layer despite the fact that they are processed from orthogonal solvents. However, the intermixing depends on the solvent that is used. In this context it has been shown that toluene does not affect the PSSA layer at all whereas chloroform does.

Additionally another water soluble polymer, PAA, has been investigated regarding the intermixing of two orthogonally soluble polymers. First results indicate that a PAA layer is neither influenced by chloroform nor toluene, which makes it insensitive to apolar solvents.

Bibliography

[1] J. S. Rutt and S. B. Maebius, "From plastics to nanotechnology: Cambridge display technology's ipo registration," *Nanotechnology Law & Business*, vol. 1, 2004.

[2] Nokia, "C7-00." http://www.nokia.com/at-de/produkte/smartphones-und-handys/c7-00/technische-daten/, 02 2012.

[3] A. Brown, C. Jarrett, D. de Leeuw, and M. Matters, "Field-effect transistors made from solution-processed organic semiconductors," *Synthetic Metals*, vol. 88, pp. 37–55, Apr. 1997.

[4] G. Horowitz, "Organic field-effect transistors," *Advanced Materials*, vol. 10, pp. 365–377, Mar. 1998.

[5] C. Newman, C. Frisbie, D. D. S. Filho, J. Brédas, P. Ewbank, and K. Mann, "Introduction to organic thin film transistors and design of n-channel organic semiconductors," *Chemistry of Materials*, vol. 16, no. 23, pp. 4436–4451, 2004.

[6] L. Chua, J. Zaumseil, J. Chang, E. C. Ou, P. K. Ho, H. Sirringhaus, and R. H. Friend, "General observation of n-type field-effect behaviour in organic semiconductors," *Nature*, vol. 434, pp. 194–199, Mar. 2005.

[7] G. Horowitz, *Organic Field-Effect Transistors*, ch. Charge Transport in Oligomers, pp. 73–101. CRC Press, 2007.

[8] G. Horowitz, R. Hajlaoui, H. Bouchriha, R. Bourguiga, and M. Hajlaoui, "Concept of 'threshold voltage' in organic field-effect transistors," *Advanced Materials*, vol. 10, no. 12, pp. 923–927, 1998.

[9] A. Ortiz-Conde, F. Garcia Sanchez, J. Liou, A. Cerdeira, M. Estrada, and Y. Yue, "A review of recent mosfet threshold voltage extraction methods," *Microelectronics Reliability*, vol. 42, pp. 583–596, April 2002.

[10] C. Kittel, *Einführung in die Festkörperphysik*. Oldenbourg Wissenschaftsverlag, Oct. 2006.

[11] L. Spiess, G. Teichert, R. Schwarzer, H. Behnken, and C. Genzel, "Methoden der röntgenbeugung," in *Moderne Röntgenbeugung*, pp. 155–216, Wiesbaden: Vieweg+Teubner, 2009.

[12] M. Krumrey, M. Hoffmann, and M. Kolbe, "Schichtdickenbestimmung mit röntgenreflektometrie," *Thin Solid Films*, vol. 115, no. 4, pp. 38–40, 2005.

[13] BASF, *Sepiolid P 200*, 2010. Productdata sheet.

[14] H.-L. Cheng, W.-Q. Lin, and F.-C. Wu, "Effects of solvents and vacancies on the electrical hysteresis characteristics in regioregular poly(3-hexylthiophene) organic thin-film transistors," *Applied Physics Letters*, vol. 94, no. 22, p. 223302, 2009.

[15] Lesker, "Diener femto." http://www.lesker.com/newweb/Vacuum_systems/Plasma_Cleaning_Systems/diener_plasma_products_femto.cfm, 10 2011.

[16] P. Pacher, A. Lex, V. Proschek, H. Etschmaier, E. Tchernychova, M. Sezen, U. Scherf, W. Grogger, G. Trimmel, C. Slugovc, and E. Zojer, "Chemical control of local doping in organic thin-film transistors: From depletion to enhancement," *Advanced Materials*, vol. 20, no. 16, pp. 3143–3148, 2008.

[17] S. K. Possanner, K. Zojer, P. Pacher, E. Zojer, and F. Schürrer, "Threshold voltage shifts in organic thin-film transistors due to Self-Assembled monolayers at the dielectric surface," *Advanced Functional Materials*, vol. 19, pp. 958–967, Mar. 2009.

[18] B. Stadlober, U. Haas, H. Gold, A. Haase, G. Jakopic, G. Leising, N. Koch, S. Rentenberger, and E. Zojer, "Orders-of-magnitude reduction of the contact resistance in short channel hot embossed organic thin film transistors by oxidative treatment of au-electrodes," *Advanced Functional Materials*, vol. 17, pp. 2687–2692, Oct. 2007.

[19] N. Jing, J. Deng, L. Yang, K. Zhao, Z. Wang, X. Cheng, Y. Hua, and S. Yin, "Photoinduced organic field-effect transistor based on poly-3-hexyl- thiophene active layer," *Journal of Nanoscience and Nanotechnology*, vol. 10, no. 3, pp. 2161–2163, 2010.

[20] H. Sirringhaus, "Reliability of organic field-effect transistors," *Advanced Materials*, vol. 21, pp. 3859–3873, 2009.

[21] S. Cho, K. Lee, J. Yuen, G. Wang, D. Moses, A. J. Heeger, M. Surin, and R. Lazzaroni, "Thermal annealing-induced enhancement of the field-effect mobility of regioregular poly(3-hexylthiophene) films," *Journal of Applied Physics*, vol. 100, no. 11, p. 114503, 2006.

[22] M. J. Joung, C. A. Kim, S. Y. Kang, K. Baek, G. H. Kim, S. D. Ahn, I. K. You, J. H. Ahn, and K. S. Suh, "The application of soluble and regioregular poly(3-hexylthiophene) for organic thin-film transistors," *Synthetic Metals*, vol. 149, pp. 73–77, Feb. 2005.

[23] S. Marchant and P. J. S. Foot, "Annealing behaviour of conductive poly(3-hexylthiophene) films," *Polymer*, vol. 38, pp. 1749–1751, Mar. 1997.

[24] B. Mattis, P. Chang, and V. Subramanian, "Effect of thermal cycling on performance of poly(3-hexylthiophene) transistors," in *Materials Research Society Symposium - Proceedings*, vol. 771, pp. 369–374, 2003.

[25] K. P. Pernstich, S. Haas, D. Oberhoff, C. Goldmann, D. J. Gundlach, B. Batlogg, A. N. Rashid, and G. Schitter, "Threshold voltage shift in organic field effect transistors by dipole monolayers on the gate insulator," *Journal of Applied Physics*, vol. 96, no. 11, p. 6431, 2004.

[26] M. G. Kane, *Organic Field-Effect Transistors*, ch. Organic Thin-Film Transistors for Flat-Panel Displays, pp. 73–101. CRC Press, 2007.

[27] J. Chang, B. Sun, D. Breiby, M. Nielsen, T. Sölling, M. Giles, I. McCulloch, and H. Sirringhaus, "Enhanced mobility of poly(3-hexylthiophene) transistors by spin-coating from high-boiling-point solvents," *Chemistry of Materials*, vol. 16, no. 23, pp. 4772–4776, 2004.

[28] H. Sirringhaus, N. Tessler, and R. Friend, "Integrated, high-mobility polymer field-effect transistors driving polymer light-emitting diodes," *Synthetic Metals*, vol. 102, pp. 857–860, June 1999.

[29] H. Etschmaier, P. Pacher, A. Lex, G. Trimmel, C. Slugovc, and E. Zojer, "Continuous tuning of the threshold voltage of organic thin-film transistors by a chemically reactive interfacial layer," *Applied Physics A*, vol. 95, pp. 43–48, Dec. 2008.

[30] T. Förster, "Die ph-abhängigkeit der fluoreszenz von naphthalinderivaten," *Zeitschrift für Elektrochemie und angewandte physikalische Chemie*, vol. 54, pp. 531–535, Dec. 1950.

[31] N. Agmon, "Elementary steps in excited-state proton transfer," *J. Phys. Chem. A*, vol. 109, no. 1, pp. 13–35, 2004.

[32] D. R. Lide, *Handbook of Chemistry and Physics*. CRC Press, 1995.

[33] R. van Langevelde and F. M. Klaassen, "Effect of gate-field dependent mobility degradation on distortion analysis in MOSFETs," *IEEE Transactions on Electron Devices*, vol. 44, pp. 2044–2052, Nov. 1997.